

On regional dynamical downscaling for the assessment and projection of temperature and precipitation extremes across Tasmania, Australia

Christopher J. White · Kathleen L. McInnes · Robert P. Cechet ·
Stuart P. Corney · Michael R. Grose · Gregory K. Holz ·
Jack J. Katzfey · Nathaniel L. Bindoff

Received: 31 July 2012 / Accepted: 2 March 2013 / Published online: 21 March 2013
© Springer-Verlag Berlin Heidelberg 2013

Abstract The ability of an ensemble of six GCMs, downscaled to a 0.1° lat/lon grid using the Conformal Cubic Atmospheric Model over Tasmania, Australia, to simulate observed extreme temperature and precipitation climatologies and statewide trends is assessed for 1961–2009 using a suite of extreme indices. The downscaled simulations have high skill in reproducing extreme temperatures, with the majority of models reproducing the statewide averaged sign and magnitude of recent observed trends of increasing *warm days* and *warm nights* and decreasing *frost days*. The *warm spell duration index* is however underestimated, while

variance is generally overrepresented in the *extreme temperature range* across most regions. The simulations show a lower level of skill in modelling the amplitude of the extreme precipitation indices such as *very wet days*, but simulate the observed spatial patterns and variability. In general, simulations of dry extreme precipitation indices are underestimated in dryer areas and wet extremes indices are underestimated in wetter areas. Using two SRES emissions scenarios, the simulations indicate a significant increase in *warm nights* compared to a slightly more moderate increase in *warm days*, and an increase in *maximum 1- and 5-day precipitation intensities* interspersed with longer *consecutive dry spells* across Tasmania during the twenty-first century.

C. J. White (✉) · S. P. Corney · M. R. Grose ·
G. K. Holz · N. L. Bindoff
Antarctic Climate and Ecosystems Cooperative Research Centre
(ACE CRC), University of Tasmania, Private Bag 80,
Hobart, TAS 7001, Australia
e-mail: Chris.White@acecrc.org.au

K. L. McInnes · J. J. Katzfey
Centre for Australian Weather and Climate Research (CAWCR),
CSIRO Marine and Atmospheric Research, Private Bag 1,
Aspendale, VIC 3195, Australia

R. P. Cechet
Geoscience Australia, GPO Box 378, Canberra,
ACT 2601, Australia

N. L. Bindoff
Institute of Marine and Antarctic Studies (IMAS), University
of Tasmania, Private Bag 129, Hobart, TAS 7001, Australia

N. L. Bindoff
Centre for Australian Weather and Climate Research (CAWCR),
CSIRO Marine and Atmospheric Research, GPO Box 1538,
Hobart, TAS 7001, Australia

Keywords Extremes · Climate change · Regional climate models · Observations · Projections · Australian climate

1 Introduction

Scientific evidence that the earth is warming is unequivocal and there is overwhelming evidence that increased concentrations of greenhouse gases, caused by human activity, are contributing to this warming (Solomon et al. 2007). Associated with this warming, other aspects of the climate system are projected to change. Changes in local weather conditions, particularly extreme events, pose a significant challenge for society and the natural environment (Senviratne et al. 2012; Burton et al. 2012) and are therefore of particular interest in the context of adaptation planning. Recent advances in extremes research have found that observations of extremes largely reflect shifts in the mean distribution (Hansen et al. 2012; Donat and Alexander 2012). However, such changes are likely to exhibit large

spatial heterogeneity (e.g. Min et al. 2011). Furthermore, weather and climate extremes are often influenced by large-scale processes and features that are not well modelled or resolved by the current generation of coupled ocean-atmosphere General Circulation Models (GCMs), contributing to uncertainty in future projections of these quantities (e.g. Meehl et al. 2004; Scaife et al. 2008), particularly at the regional level (Randall et al. 2007).

Existing studies of observed and future extremes have been undertaken globally (e.g. Tebaldi et al. 2006; Alexander et al. 2006; Kharin et al. 2007) and for the Australian region (e.g. Collins et al. 2000; Gallant et al. 2007; Alexander and Arblaster 2009). In general, these have concluded that significant changes to temperature and precipitation extremes have been observed across Australia in the past century, and that Australia is likely to see a shift towards warmer temperature extremes and increased extreme precipitation events interspersed with longer dry spells during the twenty-first century (Alexander and Arblaster 2009). However, these studies have typically been undertaken using coarse global-scale GCMs which display varied levels of skill at simulating observed trends and patterns of extremes. Kharin et al. (2007) and Kiktev et al. (2007) report that globally GCMs show reasonable skill at simulating observed extreme temperature trends but show poor model agreement for extreme precipitation patterns and trends. Similarly for Australia, Alexander and Arblaster (2009) find that both the trends and inter-annual variability of temperature extremes are well simulated by the GCMs, but that few GCMs showed significant skill at reproducing observed extreme precipitation patterns across Australia. This makes the interpretation of observed and future projected changes to extreme events difficult for practitioners at the local level where the impact of extremes is most keenly felt.

Recent observed extreme events such as the Russian heat wave in 2010 (e.g. Dole et al. 2011) and flooding in England and Wales in 2000 (e.g. Pall et al. 2011) have increased demand for information to report and attribute the causes of observed extreme events (e.g. Hegerl et al. 2004; Schiermeier 2011; Peterson et al. 2012) and to provide relevant and concise information on the potential impacts of extremes in a future non-stationary climate (IPCC 2012). This has motivated recent efforts to provide climate projections at temporal and spatial scales that are more applicable for extremes. While efforts have been made to address this on a regional scale using GCMs (e.g. Alexander and Arblaster 2009 for Australia; Sillmann and Roekner 2008 for Europe), to date little has been published on extremes at the local scale.

To address the limited ability of GCMs to simulate extremes, a commonly applied technique is dynamical downscaling in which high-resolution Regional Climate

Models (RCMs) are forced by the output of GCMs. Dynamical RCMs have been shown to simulate climate variables and related processes realistically at a range of scales and locations both across Australia (e.g. Watterson et al. 2008; Nguyen and McGregor 2009) and internationally (e.g. Boé and Terray 2007; Engelbrecht et al. 2009; Nguyen et al. 2011), often with a particular focus on resolving regional precipitation processes (e.g. Kendon et al. 2010; Berg et al. 2009). However, assessments of the performance of the dynamical downscaling process for the simulation of climate extremes have been more limited.

In this study, we aim to contribute to the knowledge of temperature and precipitation extremes by assessing aspects of the performance of dynamically downscaled climate simulations undertaken across Tasmania, Australia for the Climate Futures for Tasmania project. Tasmania is Australia's island state and features a varied maritime climate and mountainous topography. However, its relatively small size means that it is poorly resolved in global-scale GCMs where circulation changes between the east and west of the state are not distinguished (Grose et al. 2012a). Furthermore, it is located near a boundary of projected future precipitation increase to the south and decrease to the north in most GCMs (Christensen et al. 2007) and this leads to limited agreement in the sign and magnitude of future precipitation changes over the Tasmanian region between GCMs, making it an ideal location for studying and validating the performance of high-resolution regional-scale projections of climate extremes.

This paper is organized as follows. The study location, model experiments and a review of extremes metrics are given in Sect. 2. Section 3 assesses the performance of the downscaled experiments across an ensemble of six simulations with regards to their representation of extremes while Sect. 4 describes future projections. The final section provides a discussion of results and concluding comments.

2 Background and methods

2.1 Region of study

Tasmania is located 240 km south of the south-east corner of the Australian mainland (Fig. 1a), near the northern boundary of the mid-latitude belt of southern hemisphere westerlies. It is characterised by mountainous topography in much of the south and west, a plateau in the centre of the state and lowlands predominating in the north and east. The mountains create a sharp west-east mean annual precipitation gradient from more than 3,200 mm in the Western district to less than 600 mm in the East Coast lowlands district (districts are shown in Fig. 1b). Mean annual daily maximum temperatures range from ~ 12 °C in the Central

Plateau district to $\sim 17\text{ }^{\circ}\text{C}$ in the East Coast district. Although less frequent and intense as those observed in parts of the Australian mainland, temperatures as high as $42.2\text{ }^{\circ}\text{C}$ have been recorded in the state's North East and as low as $-13.0\text{ }^{\circ}\text{C}$ on the Central Plateau (Bureau of Meteorology 2012). The most extreme temperature events and worst fire danger conditions occur under the influence of strong hot dry north–westerly prefrontal winds crossing Tasmania (Mills 2005). Frontal systems are the dominant cause of precipitation in the western half of the state, while east coast low systems dominate extreme precipitation events in the northeast (Pook et al. 2010), one such example producing extreme precipitation totals of 352 mm in 1 day on the 22nd March 1974 (Bureau of Meteorology 2012).

The projections of future temperature changes across the Tasmania region from GCM simulations are broadly consistent with parts of the southern Australian mainland.

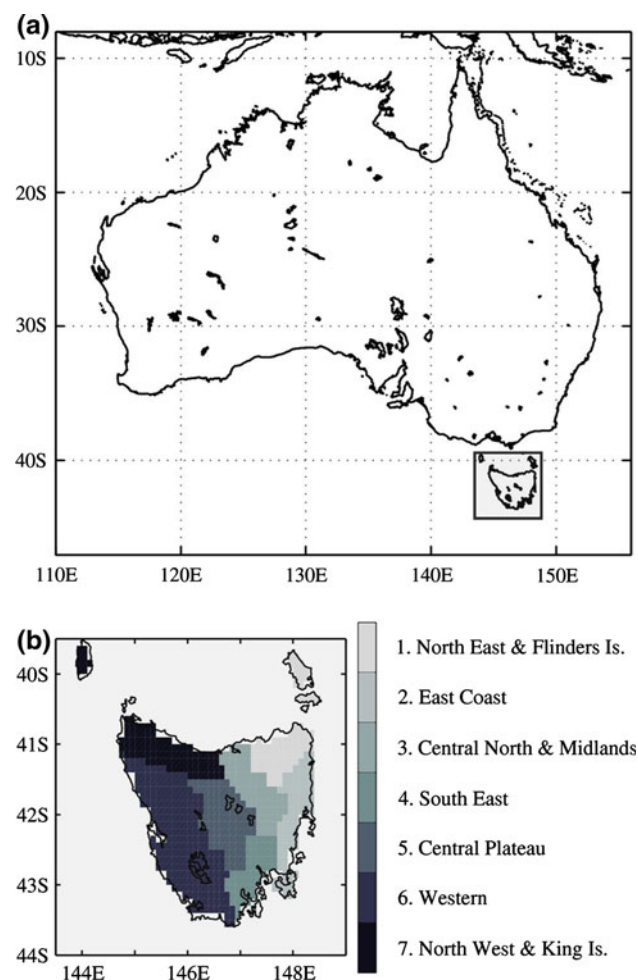


Fig. 1 Australia geographical location map showing **a** the location of the state of Tasmania, and **b** the Tasmania districts used in this study. Districts derived from the Bureau of Meteorology's Tasmanian Forecast Areas Map, available online at www.bom.gov.au/tas/forecasts/map.shtml

However, there is poor agreement on the sign and magnitude of future precipitation changes, with Tasmania lying near a boundary between the subtropics where most GCMs project a decrease in mean precipitation, and the higher latitudes where precipitation is largely projected to increase in a warming climate (Christensen et al. 2007; Suppiah et al. 2007). The exact placement of this boundary is likely to dictate both the sign and magnitude of mean and extreme precipitation changes across Tasmania. The coarse resolution of GCMs, where Tasmania is represented by between 0 and 6 grid cells (Fig. 2a shows an example using the GFDL-CM2.1 GCM), means they do not delineate the west to east gradients of precipitation or precisely define the boundary between projected future increases and decreases in precipitation.

Tasmania's location, diverse topography and varied climate over a relatively small area makes assessing the regional impacts of climate change on extreme temperature and precipitation events particularly difficult when relying solely on low-resolution GCMs. It is therefore an ideal case study location for an assessment of the performance of the new generation of high-resolution dynamically downscaled climate simulations.

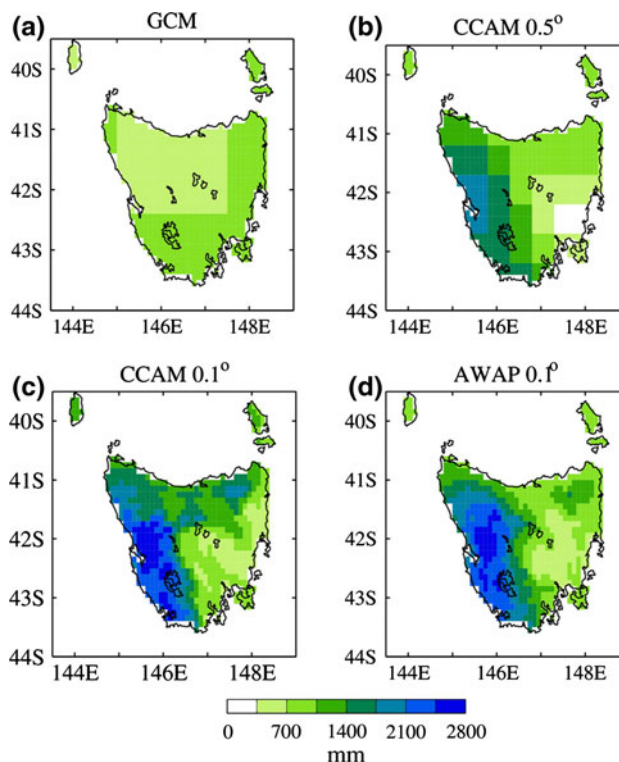


Fig. 2 Demonstration of the effects of resolution on an example variable (mean annual precipitation in mm) for Tasmania using **a** the $2.0^{\circ} \times 2.5^{\circ}$ GFDL-CM2.1 GCM, **b** the 0.5° CCAM simulations (using the same GCM), **c** the 0.1° CCAM simulations (using the same GCM), and **d** the 0.1° AWAP interpolated observations, all for 1961–1990

2.2 Models and dynamical downscaling

In this study, climate simulations for the Tasmanian region were produced by downscaling GCMs with CSIRO's Conformal Cubic Atmospheric Model (CCAM) as part of the Climate Futures for Tasmania project (Corney et al. 2010). CCAM is a global atmospheric model that uses a stretched-grid to increase the resolution over the geographic region of interest (McGregor 2005; McGregor and Dix 2008; Thatcher and McGregor 2011). Other variable resolution global atmospheric models have been shown to realistically simulate precipitation and related processes at a range of scales and locations (e.g. Berbery and Fox-Rabinovitz 2003; Fox-Rabinovitz et al. 2006; Boé and Terray 2007) as has CCAM for regional climate studies in Australia (Watterson et al. 2008; Nguyen and McGregor 2009; Chiew et al. 2010) and internationally (Lal et al. 2008; Engelbrecht et al. 2009; Nguyen et al. 2011). This study forms part of a wider body of work assessing large-scale climate processes and synoptic systems (Grose et al. 2012a, b) and future water availability (Bennett et al. 2012) using the CCAM simulations across the Tasmanian region.

Understanding model uncertainty is a key element of assessing model skill. We have used an ensemble of simulations to reduce this source of uncertainty to develop a plausible range of future changes in extremes. Five of the World Climate Research Programmes's (WCRP's) Coupled Model Intercomparison Project phase 3 (CMIP3) GCMs (Meehl et al. 2007a) were selected on the basis that they realistically simulated observed precipitation across Australia (Smith and Chandler 2009) and ENSO variability (van Oldenborgh et al. 2005) and include GFDL-CM2.0, GFDL-CM2.1, ECHAM5/MPI-OM, UKMO-HadCM3 and MIROC3.2(medres). The sixth GCM selected was the most recent Australian CMIP3 GCM; CSIRO-Mk3.5. For brevity, we refer to the downscaled GCMs as models throughout the paper.

Forcing for CCAM is typically applied in one of two ways. It can be applied at the surface boundary through the specification of bias-adjusted sea-surface temperatures and sea-ice (Katzfey et al. 2009) where the atmosphere within CCAM is able to evolve freely in response to the surface forcing. The bias-correction of the SSTs prior to their application to the CCAM model has been shown to improve the representation of the current climate (e.g. Grose et al. 2012a, b; Nguyen et al. 2011). Alternatively, CCAM can be forced using a spectral nudging technique (Thatcher and McGregor 2009) in which the surface pressure, air temperature and winds and moisture fields are perturbed at spatial scales typically greater than the size of the region of interest (in this case Tasmania) using a specified source of atmospheric data. Using spectral nudging, the atmosphere at small spatial scales is able to

evolve freely within CCAM. Both of these methods avoid the need for horizontal boundary conditions and their associated problems on limited area model domains.

While downscaling with multiple RCMs can be beneficial for capturing the uncertainty related to the downscaling model, the primary source of the climate change signal results from changes in the ocean temperatures (Dommenget 2009). Therefore, with limited resources, it was decided to only use CCAM for all the simulations, but to downscale six GCMs (to capture some of the uncertainty related to the climate change signal) and two emission scenarios (to capture some of the uncertainty related to future scenarios). The SST forcing from the host GCM is applied as a fixed correction factor for each month and so the climate change signal and the inter-annual variability in SST's from the host GCMs will be transferred to CCAM. However, as the land surface and atmosphere is not constrained by forcing from the host it can evolve independently to reflect changes in the atmosphere due to climate change.

The downscaling in this study is undertaken in two stages. In the first, CCAM, with an approximate horizontal resolution of ~ 50 km (0.5°) over the Australian continent (Fig. 2b), is forced with bias-corrected GCM sea surface temperatures (SSTs) and sea-ice concentrations. In the second stage, CCAM, at an approximate horizontal resolution of ~ 10 km (0.1°) over Tasmania (Fig. 2c), is forced with the same bias-corrected GCM SSTs and sea-ice concentrations (downscaled through the ~ 50 km simulations) as well as spectral nudging of the atmosphere from the 50 km CCAM simulations (Thatcher and McGregor 2009; Katzfey et al. 2009). The spectral nudging is necessary for the model with higher-resolution over Tasmania because the associated lower resolution of this stretched grid transformation on the opposite side of the globe means it is unable to maintain a realistic global atmosphere there (Corney et al. 2010). The downscaling approach is applied to two of the Special Report on Emissions Scenarios (SRES) experiments (Nakićenović and Swart 2000): B1 (a low-range emissions scenario) and A2 (a high-range emissions scenario).

2.3 Observations

The ability of the dynamically downscaled CCAM simulations to reproduce extreme temperature and precipitation observations and trends for the present (or validation) period of 1961–2009 is assessed using the Australian Water Availability Project (AWAP) high-resolution gridded observational dataset. AWAP is an interpolated product, created using station records across Australia (Raupach et al. 2008; Jones et al. 2009). While the AWAP dataset provides complete spatial coverage across Tasmania, some

areas of Tasmania, particularly in the west, have sparse observational station records and hence extremes in this region may be less reliable compared to areas with a denser station network (King et al. 2012). King et al. (2012) also note that AWAP tends to underestimate the intensity of extreme heavy precipitation events and overestimate the frequency and intensity of very low precipitation events. Therefore, although AWAP provides the most spatially complete dataset of daily precipitation and daily maximum and minimum temperature observations for the region, some caution in its use for evaluating the performance of the CCAM simulations is needed. In this study, we use a subset of the AWAP observations for the Tasmanian region which is interpolated from its native 0.05° grid to the CCAM 0.1° grid for direct comparison with the CCAM simulations (Fig. 2d).

2.4 Probability density functions and skill scores

Statewide and regional district area-averaged annual probability density functions (PDFs) are calculated for daily maximum temperature, daily minimum temperature, and daily precipitation. The seven regional districts (1–7) are defined in Fig. 1b. Bin sizes of 1°C for daily temperature and 1 mm for daily precipitation are used, with all daily precipitation values below 0.2 mm omitted as rates below this amount are generally not recorded in the observations. The skill of each of the six area-averaged

CCAM simulated PDFs relative to the area-averaged AWAP observed PDFs for each region for the validation period is assessed using the metric presented in Perkins et al. (2007), in which the common area between each of the PDF pairs of individual CCAM simulations and the AWAP observations is calculated. The metric is based on the cumulative minimum value of each bin used to calculate the PDFs, and the PDF skill score is then expressed as the total sum of the probability at each bin center (Perkins et al. 2007). A PDF skill score of one (zero) represents perfect (no) overlap between the two PDFs (see Perkins et al. (2007) for a formal explanation of the PDF skill score metric). PDFs of daily maximum temperature, daily minimum temperature, and daily precipitation for the 1961–2009 validation period are shown as statewide and selected regional district area-averages with corresponding PDF skill score box-whisker diagrams.

2.5 Extreme indices

Extreme events are characterised in various ways. Examples include the number of events above a selected percentile or threshold value (frequency), the amount or magnitude of the event (intensity), the percentage of time of occurrence or length of events (duration), the area impacted (spatial) or the seasonal patterns or distributions (timing). Recent studies have attempted to capture many of these parameters in a suite of simple indices to enable

Table 1 Summary of the extreme indices used in this study

Code	Index name	Definition	Units
TX90p	Warm days	Percentage of time where daily maximum temperature > the 1961–1990 90th percentile of daily maximum temperature	%
TN90p	Warm nights	Percentage of time where daily minimum temperature > the 1961–1990 90th percentile of daily minimum temperature	%
FD	Frost days	Number of days where daily minimum temperature < 0°C	Days
SU	Summer days	Number of days where daily maximum temperature > 25°C	Days
ETR	Extreme temperature range	Difference between the highest and lowest temperature values per annum	$^\circ\text{C}$
WSDI	Warm spell duration index	Annual count of days >5 consecutive days when daily maximum temperature > the 1961–1990 90th percentile	Days
R1D	Maximum 1-day precipitation	Maximum daily precipitation total	mm
R5D	Maximum 5-day precipitation	Maximum precipitation total over a consecutive 5-day period	mm
R95p	Very wet days	Number of days where daily precipitation > the 1961–1990 95th percentile of daily precipitation	Days
CDD	Consecutive dry days	Maximum number of consecutive days where daily precipitation < 1 mm	Days
CWD	Consecutive wet days	Maximum number of consecutive days where daily precipitation ≥ 1 mm	Days
SDII	Simple daily intensity index	Ratio of annual wet-day total precipitation to annual number of wet-days	mm d^{-1}

Extreme temperature indices calculated using daily maximum and minimum temperature ($^\circ\text{C}$); extreme precipitation indices calculated using daily precipitation totals (mm). Index definitions can be viewed in full at <http://ccma.seos.uvic.ca/ETCCDI/>

consistent and comparable analyses to be undertaken. A suite of twenty-seven definitions of extreme temperature and precipitation indices (Zhang et al. 2011) were developed for the measurement and characterisation of extreme climate variability and climate change using observations and modelled projections by the CCI/CLIVAR/JCOMM Expert Team on Climate Change Detection and Indices (ETCCDI) panel.

A subset of the ETCCDI extreme indices—six precipitation and six temperature—are used in this study to assess the performance of the CCAM simulations at simulating temperature and precipitation extremes across Tasmania for the 1961–2009 validation period and to demonstrate future projected changes in extreme events across the state up to 2099. The twelve indices used in this study are summarised in Table 1 and are referred to hereafter by their index codes. The indices are selected to focus on different aspects of the temperature and precipitation extremes. The indices compare contrasting parts of the distributions (e.g. warm night time extremes such as TN90p and hot day time extremes such as TX90p), cover different metrics of extremes such as magnitude (e.g. R1D), frequency (e.g. R95p) and duration (e.g. CWD), and, in some cases, allow for an inter-comparison of the indices themselves (e.g. percentile-based indices such as TX90p vs. fixed threshold indices such as SU). The indices are also selected for their general applicability to the Tasmanian region and usability within the wider communities. In addition, a larger set of the ETCCDI extreme indices for the Tasmanian region can be seen in White et al. (2010a).

The extreme indices are calculated for each of the downscaled 0.1° CCAM simulations independently and the results averaged across the six models to provide a multi-model mean (referred to hereafter as CCAM–MMM) and these are compared to the 0.1° AWAP interpolated observations (referred to hereafter as AWAP). It is noted however that while the central estimate from multiple simulations generally provides more robust information than from any single model (Meehl et al. 2007b), there remains a range of uncertainty with it. Therefore, where applicable the CCAM–MMM time series for each index are presented with a minimum and maximum range calculated across the six models.

2.6 Trends

Decadal trends for each of the temperature and precipitation extreme indices are calculated using simple linear Ordinary Least Squares (OLS) regression following Alexander and Arblaster (2009). Goodness of fit of the regression is assessed using the R^2 correlation coefficient and trend significance is estimated using two methods: (a) significance of the slope coefficient, and (b) slope significance

using a non-parametric Mann–Kendall test (Mann 1945; Kendall 1975). The non-parametric test was used in conjunction with the standard regression test to test against departures of assumptions, as well as to safe-guard against possible extreme effects of outliers, if present. All tests were performed at the 5 % level. In all cases, the differences between the sets of test results were minimal and in most cases identical, therefore we concluded that linear regression was appropriate for this study. For each index, trends are calculated for each grid cell for the AWAP observations and for each of the six CCAM simulations. Future projections are shown for all districts as area-averaged decadal trends per CCAM simulation up to 2099 with ± 90 % confidence intervals and trend significance, and as CCAM–MMM area-averaged decadal trends.

3 Downscaling performance of extremes

3.1 Validation of the downscaled simulations

In the global-scale host GCMs, the orography of Tasmania is poorly represented leading to weak spatial correlation between variables from the host GCM and observations (Corney et al. 2010), particularly for the spatial distribution of precipitation (Fig. 2a). In the downscaled 0.5° and 0.1° CCAM simulations, interaction between rain-producing systems and model orography through mechanisms such as orographic lifting leads to more realistic results (Fig. 2b, c). This is demonstrated in Table 2 where the spatial correlation of the 0.1° CCAM simulation of mean precipitation from GFDL-CM2.1 with the AWAP observations for the same period has a statewide correlation coefficient of 0.86 compared with 0.00 for the native GCM resolution. The slightly higher value of 0.88 for the 0.5° simulation compared to the 0.1° simulation reflects the smoother topography in the 0.5° simulations. Similarly, for daily maximum and daily minimum temperatures, spatial correlations between the 0.1° CCAM simulation (forced by GFDL-CM2.1 in this example) and AWAP are considerably higher than those between the host GCM and AWAP.

Table 2 Spatial correlations between GFDL-CM2.1 and the 0.1° AWAP observations at three resolutions: GFDL-CM2.1 native 2.0° × 2.5° GCM resolution, CCAM downscaled 0.5° resolution, and CCAM downscaled 0.1° resolution, all for 1961–1990

Model resolution	Mean daily maximum temperature	Mean daily minimum temperature	Mean precipitation
GCM	−0.15	0.43	0.00
0.5°	0.59	0.83	0.88
0.1°	0.94	0.90	0.86

The correlation coefficients of GFDL-CM2.1 are highly representative of the six 0.1° CCAM simulations (not shown).

In addition to the spatial correlations of the climatologies for the validation period, the capacity of the CCAM simulations to reproduce the full PDFs of observed mean precipitation, daily maximum and daily minimum temperature is an equally important test of the fidelity. Figure 3 shows the general shape and skew of the

Tasmanian area-averaged AWAP daily maximum and minimum temperature PDFs to be well simulated by the six CCAM models, with consistently high CCAM–MMM PDF skill scores >0.89 for daily maximum temperature (Fig. 4a) and >0.91 for daily minimum temperature (Fig. 4b) across the districts (see Fig. 1b for district definitions). PDF skill scores of daily maximum temperature are slightly more varied across the regions than daily minimum temperature, with the lower lying districts

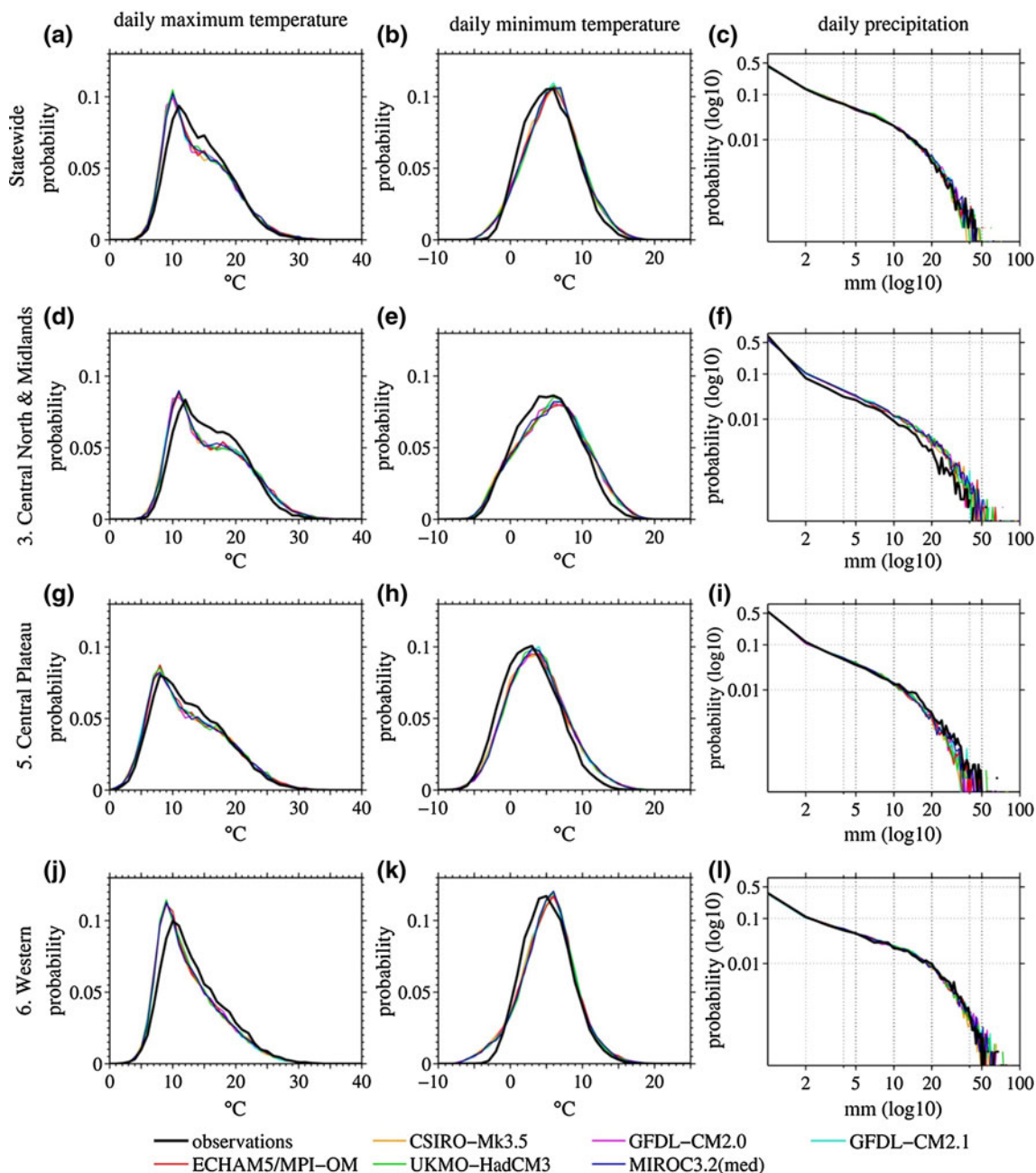


Fig. 3 Statewide and selected district area-averaged probability density functions of **a** daily maximum temperature, **b** daily minimum temperature, and **c** daily precipitation for the 0.1° AWAP

observations (*bold black lines*) and for each of the 0.1° CCAM simulations (*thin coloured lines*) (1961–2009). Numbered Tasmania districts (1–7) are defined in Fig. 1b

typically exhibiting slightly lower daily maximum temperature PDF skill scores. The area-averaged daily mean precipitation PDFs from CCAM show a slight tendency to overestimate the lower end of the distribution combined with a tendency to underestimate the magnitude of the more extreme precipitation events compared to the AWAP PDFs (Fig. 3c), however the overall PDF skill scores are high (Fig. 4c). Considering agreement between the area-averaged CCAM and AWAP mean precipitation PDFs, the majority of districts display CCAM–MMM PDF skill scores >0.95 . The lowest skill score of ~ 0.82 (Fig. 4c) is due to overestimation of extreme precipitation occurring over the Central North and Midlands district, which is a region that has the largest mean precipitation bias in the CCAM simulations (Grose et al. 2010).

It is interesting to note that the area-averaged skill scores are generally higher for the mean precipitation PDFs than for the daily maximum and minimum temperature PDFs across the majority of the districts. While there is no physical basis to fully explain this, it is likely that the PDF skill score method of Perkins et al. (2007) is more appropriate for variables that are close to normally distributed such as temperature, than those that are far from normally distributed such as precipitation. Notwithstanding this however, the high PDF skill scores across the three variables are indicative of the overall high skill of the six CCAM simulations at capturing the observed PDFs, which is reflected in the shape of the PDFs (Fig. 3) and the tight grouping of the skill scores for each of the different Tasmanian regions (Fig. 4).

3.2 Validation of decadal trends

The observed mean temperature trend over the state of Tasmania is ~ 0.1 °C per decade over the 1961–2009 period (Grose et al. 2010), which suggests that observed trends in the extreme indices may also be evident. Trends over the validation period are calculated for each of the six

CCAM simulations independently and compared to those from the AWAP observations. Significance is tested at the 5 % level using the Mann–Kendall test (Mann 1945; Kendall 1975). Strong statewide area-averaged statistically significant positive trends of 0.5 %/decade for TX90p (Fig. 5a) and 0.36 %/decade for TN90p (Fig. 5b) and a strong statistically significant negative trend of -1.3 days/decade for FD (Fig. 5c) are observed in the AWAP observations over 1961–2009 indicating a progressively warming climate over the past half-century across Tasmania. The CCAM simulations reproduce the observed trends with a high level of skill with all models simulating the correct sign and, mostly, the significance of the trends. Importantly, the CCAM–MMM simulations of each extreme index for the validation period (with the exception of ETR and CDD) fall within the 95 % confidence intervals of the corresponding trend estimated from the AWAP observations (Fig. 5). Since rising greenhouse gases and tropospheric aerosols are the key forcing mechanism for the trends in the climate model simulations, this suggests that trends in the observed indices may be attributed to rising greenhouse gases and aerosols.

In terms of the skill of the individual CCAM simulations in representing the observed trends in temperature indices (except ETR; Fig. 5e), GFDL-CM2.0, GFDL-CM2.1 and ECHAM5/MPI-OM simulate the correct sign and a similar magnitude to the observed extreme temperature trends, whereas CSIRO-Mk3.5, UKMO-HadCM3 and MIROC3.2(medres) show reduced ability at simulating the correct trends with mixed signs and/or magnitudes. For example, the GFDL-CM2.0, GFDL-CM2.1 and ECHAM5/MPI-OM models simulate significant positive trends of 0.5, 0.7 and 0.6 %/decade in TX90p respectively for the validation period in close agreement with AWAP. In comparison, the CSIRO-Mk3.5 and UKMO-HadCM3 models capture the direction and significance of warming trends evident in the observed FD index, but show reduced skill at simulating the warmer extreme indices of TX90p, SU and

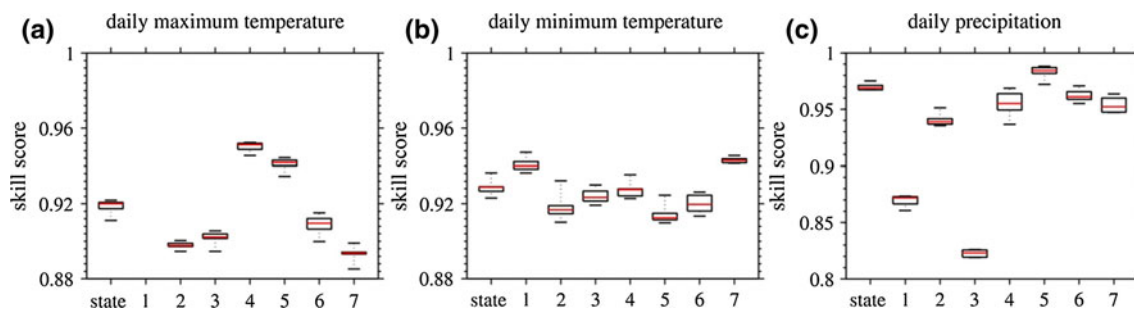


Fig. 4 Statewide and district area-averaged annual PDF skill score box-whisker diagrams of **a** daily maximum temperature, **b** daily minimum temperature, and **c** daily precipitation for the 0.1° CCAM simulations relative to the 0.1° AWAP observations (1961–2009). Red horizontal bar in the centre of each box is the CCAM multi-

model mean PDF skill score. Upper and lower bars show the 75th and 25th percentiles of the six model ensemble and the whiskers show the maximum and minimum values from across the six models. Numbered Tasmania districts (1–7) are defined in Fig. 1b

WSDI. Arguably, the worst performing model for the extreme temperature indices is MIROC3.2(medres) which finds no statistically significant trends for any of the extreme temperature indices (the only model to not do so) and underestimates the magnitudes of the observed trends in each case. The observed ETR flat trend, however, is generally not simulated well by any of the CCAM down-scaled models, which is reflective of the models over-

representing the variance associated with absolute maximum and minimum extreme temperature magnitudes (Fig. 5e).

With respect to observed trends in the precipitation indices, only CWD (Fig. 5k) is statistically significant with a statewide average trend of -0.6 days/decade for the 1961–2009 validation period. Given the weakness of the observed trends across the majority of the precipitation

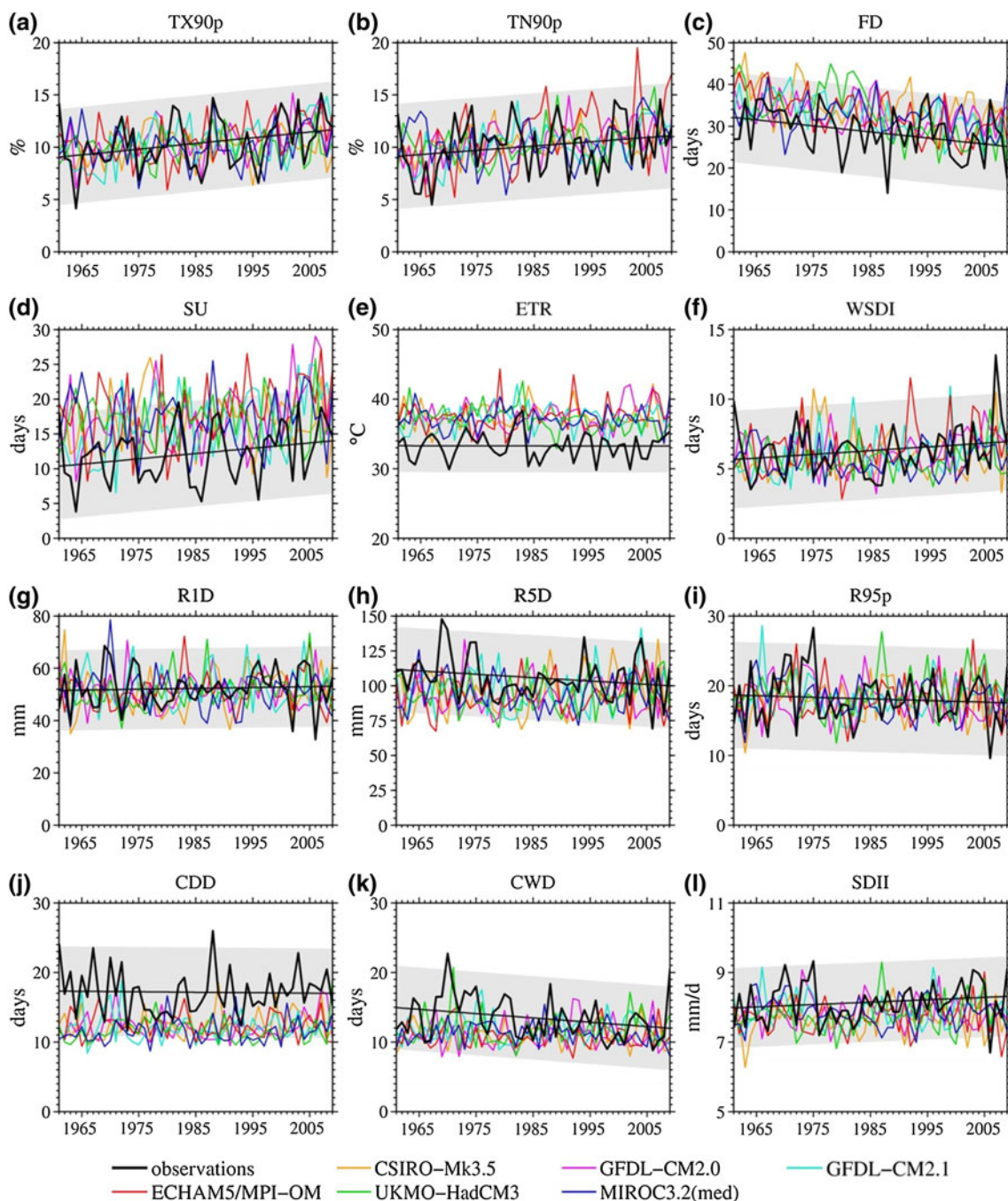


Fig. 5 Statewide area-averaged time series (1961–2009) for the 0.1° AWAP observations (*bold black lines*) and for each of the 0.1° CCAM simulations (*thin coloured lines*) for the extreme indices used

in this study (definitions shown in Table 1). *Thin black lines* show the 0.1° AWAP observed linear trend for 1961–2009 and *grey shading* shows the 90 % confidence interval of the trend

indices (Fig. 5g–l), it is perhaps not surprising that none of the CCAM simulations simulate extreme precipitation trends statewide with any significance. Of the six CCAM simulations, ECHAM5/MPI-OM is the only model to correctly simulate all of the observed signs of the extreme precipitation trends, and is also the only model to capture the observed increasing trend of R1D (Fig. 5g) and the decreasing trend of R5D (Fig. 5h), although confidence at the 90 % level is low. ECHAM5/MPI-OM is also one of only two models (with GFDL-CM2.1) to simulate the flat or decreasing observed trends for both CDD (Fig. 5j) and CWD (Fig. 5k). For other models, the trends are generally mixed across the extreme precipitation indices, with some disagreement in both the signs and magnitudes of the trends for the validation period, which is broadly consistent with the higher noise-to-signal ratio and larger confidence intervals compared to the temperature extremes.

3.3 Validation of extreme temperature climatologies

The previous sections have shown that the CCAM simulations capture the spatial distributions of PDFs and trends over broad regions of Tasmania. Here we examine the spatial patterns (Fig. 6) and the statewide area-averages differences between of the extreme indices of the CCAM simulations with respect to the AWAP observations (Table 3). There is generally good agreement between the CCAM simulations and the AWAP observations for the extreme temperature indices of TX90p (Fig. 6a), TN90p (Fig. 6b) and SU (Fig. 6d) although the CCAM simulations tend to overestimate SU in the East Coast and North East and Flinders Island districts compared to AWAP. Historically this area of the state has observed some of the most extreme temperature events, including the highest recorded

statewide temperature of 42.2 °C on 30 January 2009 at Scamander in the state's north-east (Bureau of Meteorology 2012). The spatial variance shown in the CCAM–MMM for SU in this region consistently forces the statewide area-average values well above the observed values (Fig. 5d). TX90p (Fig. 6a; Table 3) and TN90p (Fig. 6b; Table 3) are generally more consistent, with prominent differences being limited to some coastal regions in the north and low lying areas in the east for TX90p and the coastal regions of the North West and North East districts and the mountainous Western district for TN90p.

For the colder extremes, the CCAM–MMM shows mixed skill at simulating the spatial patterns of FD (Fig. 6c) compared to AWAP. The highest frequencies of observed cold extremes occur at higher elevations encompassing the Central Plateau district, but the CCAM–MMM underestimates FD in this region for the validation period. The CCAM–MMM also overestimates FD in the Western and North West districts (Fig. 6c) leading to strong statewide overestimates (Fig. 5c), driven largely by a bias over the summer DJF season.

The CCAM–MMM underestimates the WSDI across most districts compared to AWAP (Fig. 6f) and Table 3 indicates that this underestimation is fairly uniform across the seasons. However, the ability of CCAM to simulate consecutive extreme temperature days is evident in the narrow multi-model spread seen in the individual CCAM statewide averages (Fig. 5f). In contrast though, variance in ETR is generally overestimated in the CCAM–MMM across almost all of the state (Fig. 6e) producing a statewide area-average difference of 4.1 °C compared to the AWAP observations (Fig. 5e; Table 3). This is particularly strong in the autumn SON and winter DJF seasons, indicating reduced skill by the CCAM downscaled models at

Table 3 Statewide area-averaged annual and seasonal multi-model mean differences between the 0.1° CCAM simulations and the 0.1° AWAP observations (CCAM minus AWAP) for the extreme indices used in this study (definitions shown in Table 1) for 1961–2009

Index	Annual	DJF	MAM	JJA	SON
TX90p	0.0 (−0.3/0.4)	−0.1 (−0.9/0.6)	0.4 (−0.1/1.1)	0.4 (−0.6/1.4)	0.1 (−0.4/0.7)
TN90p	0.4 (0.2/1.0)	−0.2 (−0.8/1.1)	1.3 (0.8/1.9)	0.0 (−0.9/1.1)	0.4 (−0.2/1.2)
FD	4.4 (3.7/6.6)	1.0 (0.9/1.1)	1.6 (1.4/1.9)	−1.6 (−2.1/−0.3)	3.4 (3.2/4.0)
SU	5.0 (4.4/5.9)	5.0 (4.5/5.9)	−0.5 (−0.8/−0.3)	0.0 (0.0/0.0)	0.5 (0.4/0.6)
ETR	4.1 (3.8/4.4)	2.7 (2.4/3.1)	0.9 (0.6/1.2)	1.2 (0.9/1.3)	3.3 (2.9/3.6)
WSDI	−0.3 (−0.7/0.1)	−0.2 (−0.3/0.0)	−0.3 (−0.5/0.0)	−0.6 (−0.8/−0.4)	0.2 (0.0/0.3)
R1D	−0.8 (−1.4/−0.1)	−4.0 (−5.3/−2.9)	0.3 (−2.0/2.3)	−0.3 (−0.8/0.6)	2.1 (0.9/3.4)
R5D	−11.3 (−12.9/−9.0)	−12.7 (−14.0/−11.1)	−5.2 (−8.0/−3.3)	−9.2 (−10.5/−5.9)	−4.0 (−6.7/−1.5)
R95p	0.2 (−0.2/0.7)	−0.1 (−0.4/0.1)	0.4 (0.2/0.8)	−0.2 (−0.3/0.1)	0.1 (−0.2/0.4)
CDD	−5.1 (−5.6/−4.7)	−4.0 (−4.3/−3.6)	−4.0 (−4.3/−3.8)	−2.4 (−2.6/−2.2)	−2.2 (−2.5/−1.9)
CWD	−2.2 (−2.5/−1.6)	−0.6 (−0.7/−0.3)	−0.4 (−0.8/0.0)	−1.6 (−2.1/−1.2)	−1.6 (−1.9/−1.3)
SDII	−0.4 (−0.5/−0.3)	−1.3 (−1.4/−1.1)	−0.3 (−0.5/0.0)	0.1 (0.0/0.3)	−0.2 (−0.4/0.0)

Differences are shown with a minimum and maximum range (in brackets) calculated independently across the six models

simulating the magnitude of the single-most extreme temperature values in any given year.

3.4 Validation of extreme precipitation climatologies

Unlike extreme temperature events that typically occur over wide areas, extreme precipitation events are typically localised phenomena occurring over relatively short time and space scales, driven by a complex interaction of temperature, moisture, winds and topography. Although there is generally good agreement between the CCAM–MMM and AWAP across the six extreme precipitation indices, some indices display significant spatial differences to the mean patterns in some areas of the state (Fig. 6g–l). These differences are likely to be related to the different climate drivers of extreme events, although limitations of observed precipitation extremes in the AWAP dataset noted earlier, particularly in areas of sparse station coverage, should not be overlooked. The Western, Central North and East Coast districts for example are more prone to intense precipitation events (and subsequently to potential flooding) than the rest of the state, exhibiting considerable inter-annual variability. The north–east of the state in particular has recorded some of the state’s most extreme precipitation events (White et al. 2010a; Bureau of Meteorology 2012). Such rare events are dominated by large-scale meteorological drivers such as cutoff lows and frontal systems and the influence of these systems can vary markedly over relatively small distances. For example, cutoff lows accounted for >50 % of precipitation totals in the East Coast district between April and October (calculated using the Bureau of Meteorology observational record for 1981–2009), whereas Launceston in the Central North district, despite being less than 100 km from the East Coast

district, received nearly half of its total precipitation from frontal systems observed for the same period (Pook et al. 2010).

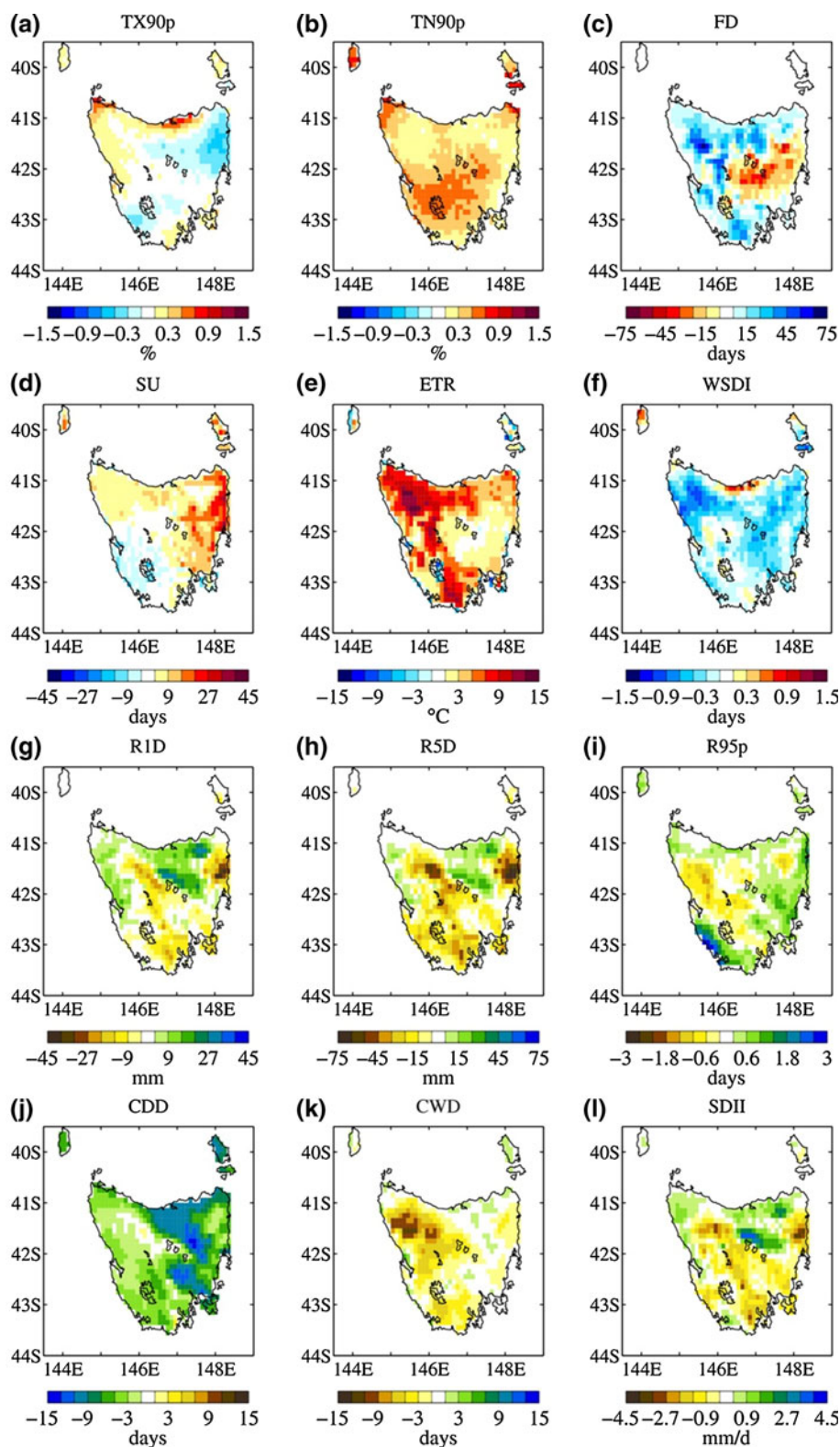
GCMs generally underestimate cutoff lows in southeast Australia and the associated features such as atmospheric blocking over the Tasman Sea and the split jet structure (e.g. Katzfey and McInnes 1996; McIntosh et al. 2008). The CCAM simulations also show these biases including an underestimate of the incidence of cutoff lows, but the biases are generally smaller than GCMs (Grose et al. 2012a). Consequently, although CCAM simulates mean annual precipitation with considerable skill across the whole of the state (Grose et al. 2010), the simulation of extreme precipitation indices of R1D (Fig. 6g) and R5D (Fig. 6h) is underestimated by the CCAM–MMM by ~45 mm and ~75 mm respectively in the East Coast district. This is related to a northward bias in the central latitude of cutoff lows in the CCAM simulations, which produces an underestimation of the associated precipitation over Tasmania for April to October (Grose et al. 2012a). Correspondingly, the overestimation of extreme precipitation totals across the Central North and Midland districts may be explained by too many frontal systems in the CCAM simulations relative to observations. Across the remainder of the state, the CCAM simulations show improved skill for R1D (Fig. 6g) and R5D (Fig. 6h) with the annual statewide average of the CCAM–MMM closely resembling the AWAP observations (Table 3). This is due, in part, to CCAM’s ability to simulate the regional impact of cutoff lows across Tasmania (Grose et al. 2012a). It is also worth noting that the generally low variability in R1D and R5D in the AWAP observations during the 1975–1995 period (Fig. 5g, h) coincides with a general decline in precipitation in southeast Australia seen in observations

Table 4 Statewide area-averaged decadal trends calculated for the 0.1° CCAM simulations (single models) for the extreme indices used in this study (definitions shown in Table 1, per decade)

Index	CSIRO-Mk3.5	GFDL-CM2.0	GFDL-CM2.1	ECHAM5/MPI-OM	UKMO-HadCM3	MIROC3.2(medres)
TX90p	1.63 (±0.14)	1.37 (±0.14)	1.29 (±0.15)	1.57 (±0.16)	1.46 (±0.14)	1.51 (±0.15)
TN90p	2.44 (±0.18)	1.78 (±0.17)	1.84 (±0.15)	1.89 (±0.20)	2.32 (±0.18)	1.98 (±0.18)
FD	-2.15 (±0.15)	-1.82 (±0.16)	-1.63 (±0.15)	-1.92 (±0.20)	-1.97 (±0.18)	-2.03 (±0.14)
SU	2.83 (±0.33)	2.48 (±0.34)	2.04 (±0.34)	2.47 (±0.42)	2.33 (±0.35)	2.55 (±0.37)
ETR	-0.07 (±0.12)	0.06 (±0.13)	0.14 (±0.13)	0.01 (±0.13)	0.08 (±0.14)	0.01 (±0.13)
WSDI	0.98 (±0.11)	0.72 (±0.16)	0.86 (±0.14)	0.90 (±0.16)	0.99 (±0.16)	0.94 (±0.18)
R1D	0.85 (±0.96)	0.91 (±0.70)	0.36 (±0.85)	1.19 (±0.77)	1.01 (±1.05)	0.42 (±0.63)
R5D	0.32 (±1.86)	0.61 (±1.11)	0.25 (±1.34)	0.99 (±1.34)	1.16 (±1.63)	-0.21 (±1.26)
R95p	0.18 (±0.20)	0.15 (±0.23)	0.29 (±0.23)	0.11 (±0.21)	0.25 (±0.24)	0.30 (±0.22)
CDD	-0.04 (±0.15)	0.11 (±0.17)	0.02 (±0.17)	0.18 (±0.14)	0.09 (±0.15)	0.09 (±0.14)
CWD	0.13 (±0.15)	-0.06 (±0.14)	-0.06 (±0.18)	-0.17 (±0.11)	0.11 (±0.17)	-0.12 (±0.12)
SDII	0.03 (±0.04)	0.05 (±0.04)	0.05 (±0.04)	0.07 (±0.04)	0.05 (±0.04)	0.09 (±0.04)

Trends are shown for the SRES A2 scenario for 2010–2099. Bold values signify trend significance at the 5 % level with ±90 % confidence intervals (in brackets)

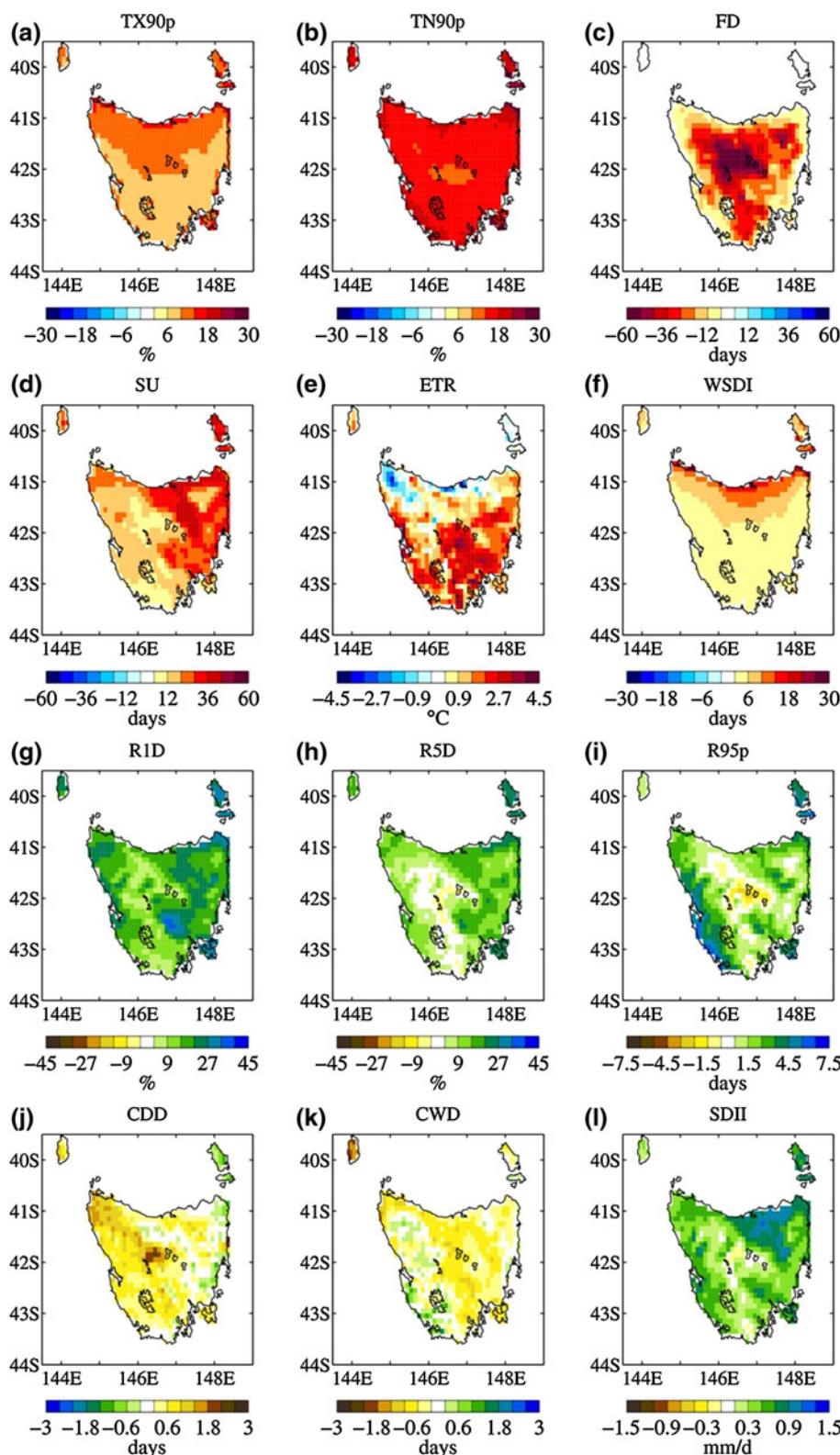
Fig. 6 Multi-model mean differences between the 0.1° CCAM simulations and the 0.1° AWAP observations (CCAM minus AWAP) for the extreme indices used in this study (definitions shown in Table 1) for 1961–2009. *Blue-to-red colourbars* denote hot extreme temperature indices using daily maximum temperature, *red-to-blue colourbars* denote cold extreme temperature indices using daily minimum temperature, *brown-to-blue/green colourbars* denote wet extreme precipitation indices and *blue/green-to-brown colourbars* denote dry extreme precipitation indices both using daily precipitation totals, where positive values signify a multi-model mean overestimate and negative values show a multi-model mean underestimate



(e.g. Murphy and Timbal 2008). The CCAM–MMM also shows skill in simulating the high inter-annual variability of R95p (Fig. 5i) by capturing the frequency of the extreme precipitation events with a statewide area-average of

between 10 and 30 days per annum across the models for the validation period. This simulated variability is strongly influenced by the most extreme precipitation events occurring in these Western, North east and East Coast

Fig. 7 Multi-model mean projected future anomalies (2070–2099 relative to 1961–1990) for the extreme indices used in this study (definitions shown in Table 1) using the 0.1° CCAM simulations for the SRES A2 scenario. As for Fig. 3, *blue-to-red colourbars* denote hot extreme temperature indices, *red-to-blue colourbars* denote cold extreme temperature indices, *brown-to-blue/green colourbars* denote wet extreme precipitation indices and *blue/green-to-brown colourbars* denote dry extreme precipitation indices, where positive values signify multi-model mean increasing future trends and negative values show multi-model mean decreasing future trends



districts (White et al. 2010b) and is robust across the seasons (Table 3).

The CCAM simulations show lower skill at resolving longer duration precipitation events with the CCAM–

MMM of CCD (Figs. 5j, 6j) and CWD (Figs. 5k, 6k) both underestimated compared to AWAP across all seasons (Table 3), particularly in the eastern districts for CDD and the western districts for CWD. Crucially, the longest

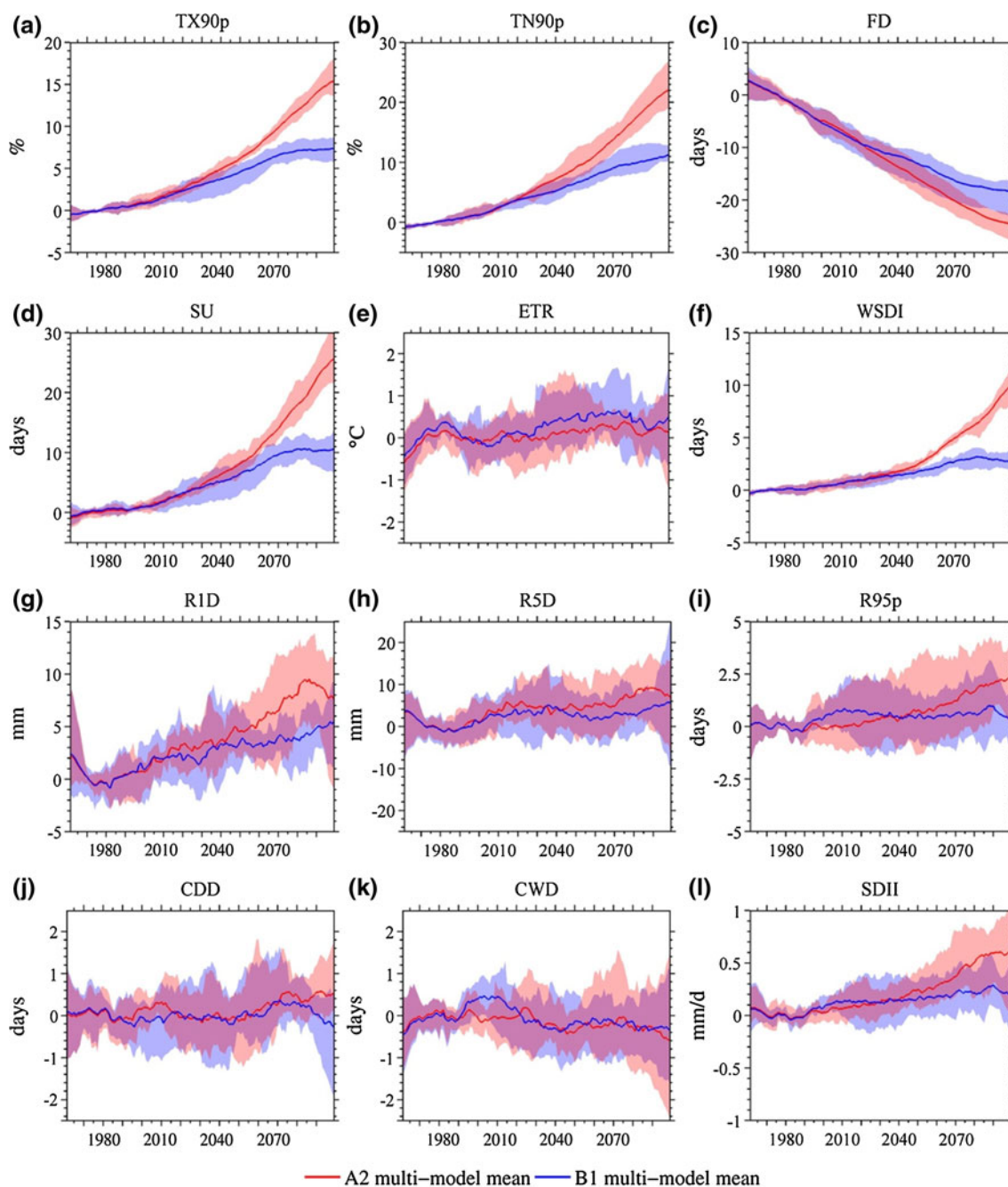


Fig. 8 Statewide area-averaged time series anomalies (1961–2099 relative to 1961–1990) of the 0.1° CCAM simulations for the extreme indices used in this study (definitions shown in Table 1). Multi-model means (*bold lines*) of the six CCAM downscaled models are shown

for the SRES B1 (*blue*) and A2 (*red*) scenarios with the maximum and minimum spread from across the six models (*shading*). Time series are smoothed with an eleven-year running mean

observed dry spells typically occur in the lower lying areas in the eastern half of the state and the longest wet spells are observed in the western half of the state. This suggests that that the CCAM simulations have reduced skill at simulating the autocorrelation (i.e. the temporal sequencing) of consecutive extreme events in regions where the most extreme values are observed, leading to the east–west bias evident in many of the precipitation indices. This is driven

by the limitations of CCAM to accurately model the larger proportion of extreme precipitation totals in the western half of the state compared to the east as well as the simulation of the dominant synoptic systems that bring extreme precipitation events to these regions. This is supported by results for SDII, the ratio of annual total wet-day precipitation to annual number of wet-days (Fig. 6l), the latter of which is overestimated by the CCAM simulations

in the Central North and North East districts (White et al. 2010b; Bennett et al. 2010).

While the extremes indices for some variables exhibit biases, the large reduction in biases compared to the parent GCMs, together with the increase in spatial resolution and extra information regarding topography and land surface, mean that there is increased confidence that the dynamics of extremes are reasonably well simulated. Therefore, it is expected that the climate change signal in extreme events at the regional scale is more reliable than the GCMs.

4 Future projections

The previous sections have shown that the CCAM simulated extreme temperature and precipitation PDFs, trends and spatial patterns compare well on balance to the AWAP observations across the validation period, suggesting that the future projections should be plausible representations of future changes across Tasmania. The future projections of the extreme temperature and precipitation indices defined in Table 1 are shown as CCAM–MMM anomalies spatially for 2070–2099 relative to 1961–1990 for the SRES A2 scenario (Fig. 7) and as statewide area-averaged time series for 1961–2099 relative to 1961–1990 for the SRES B1 (blue) and A2 (red) scenarios (Fig. 8) with a minimum and maximum range calculated across the six models. Time series are smoothed with an eleven-year running mean to reduce the inter-annual variability.

4.1 Future extreme temperature projections

Increases are projected in five of the six extreme temperature indices (Fig. 7a–f). For SU, a larger increase is projected at lower elevations, particularly in the Central North and Midlands district with many regions projected to experience up to a three-fold increase in the number of SU relative to 1961–1990 for the SRES A2 scenario (Fig. 8d). For the SRES B1 scenario the rate of rise slows abruptly in the latter half of the century. Projected decreases in FD (Fig. 7c) are consistent with an overall warming trend. The most dramatic decreases of up to 60 days per annum are projected by the CCAM–MMM SRES A2 scenario at the higher elevation Central Plateau district, which currently experiences the highest number of frosting events. Statewide, this corresponds to a decrease of ~ 24 days per annum on average for the SRES A2 scenario and ~ 18 days per annum on average for the SRES B1 scenario (Fig. 8c).

A comparison of the projected statewide averages of TX90p (Fig. 8a) and TN90p (Fig. 8b) indicates that the frequency of TX90p increases at a slightly lower rate proportionally than increases in TN90p. Progressively

throughout the 21st century, there is a greater percentage of time where maximum daily maximum temperatures are above the baseline 90th percentile (an increase of $\sim 15\%$ statewide for the SRES A2 scenario by the end of the century) compared to a more substantial change in the percentage of time where maximum daily minimum temperatures are above the corresponding baseline 90th percentile values (an increase of $\sim 22\%$ statewide for the SRES A2 scenario). In both cases, the greatest changes are projected in coastal regions, particularly in the North East and Flinders Island and North West and King Island districts. The changes to TN90p are however noticeably lower than the global (Tebaldi et al. 2006) and Australia-wide (Alexander and Arblaster 2009) projected increases of $\sim 40\%$ by the end of the twenty-first century, which is likely due to the maritime nature of the Tasmanian climate and the moderating effect of the Southern Ocean. The asymmetry evident in the trends of daily maximum temperature compared to daily minimum temperature is influenced by the changes in cloud, soil moisture, precipitation and water vapour, which are in turn influenced by greenhouse and aerosol forcings (Dai et al. 1999).

Changes to ETR (Fig. 7e) are not consistent across the state, with a projected increase of $\sim 3\text{ }^\circ\text{C}$ across much of the southern half of the state being offset by a decrease of $\sim 1\text{ }^\circ\text{C}$ in the North West including King Island and the North East including Flinders Island districts. This is, despite the increase in both mean and maximum temperatures across the state. These regions are directly adjacent to a projected enhancement of the East Australian Current, which is likely to result in higher SSTs directly adjacent to the northern and eastern coastlines of Tasmania (Cai et al. 2005), with the greatest increases in autumn and winter (Grose et al. 2010). This seasonally-varying change in SSTs immediately adjacent to the islands may have a moderating influence on ETR. The region of the largest increase in ETR is the east and south of the state, which also experiences the hottest temperatures and greatest fire-weather danger during conditions of hot, dry pre-frontal north–westerly winds (Fox-Hughes 2008). WSDI shows a general enhancement compared to the baseline 1961–1990 spatial distribution, with an increased average duration of up to 30 days per annum for the SRES A2 scenario being particularly apparent in the North West and King Island, Central North and North East and Flinders Island districts for 2070–2099 (Fig. 7f). This pattern corresponds spatially with the projected changes to TX90p (Fig. 7a) and other extreme indices such as tropical nights (where daily minimum temperatures are $>20\text{ }^\circ\text{C}$) (White et al. 2010b; not shown) which may also be influenced by the increase in local SSTs from an enhanced East Australian Current interacting with the local climate processes. Statewide, the averaged WSDI projected increase of ~ 10 days (Fig. 8f)

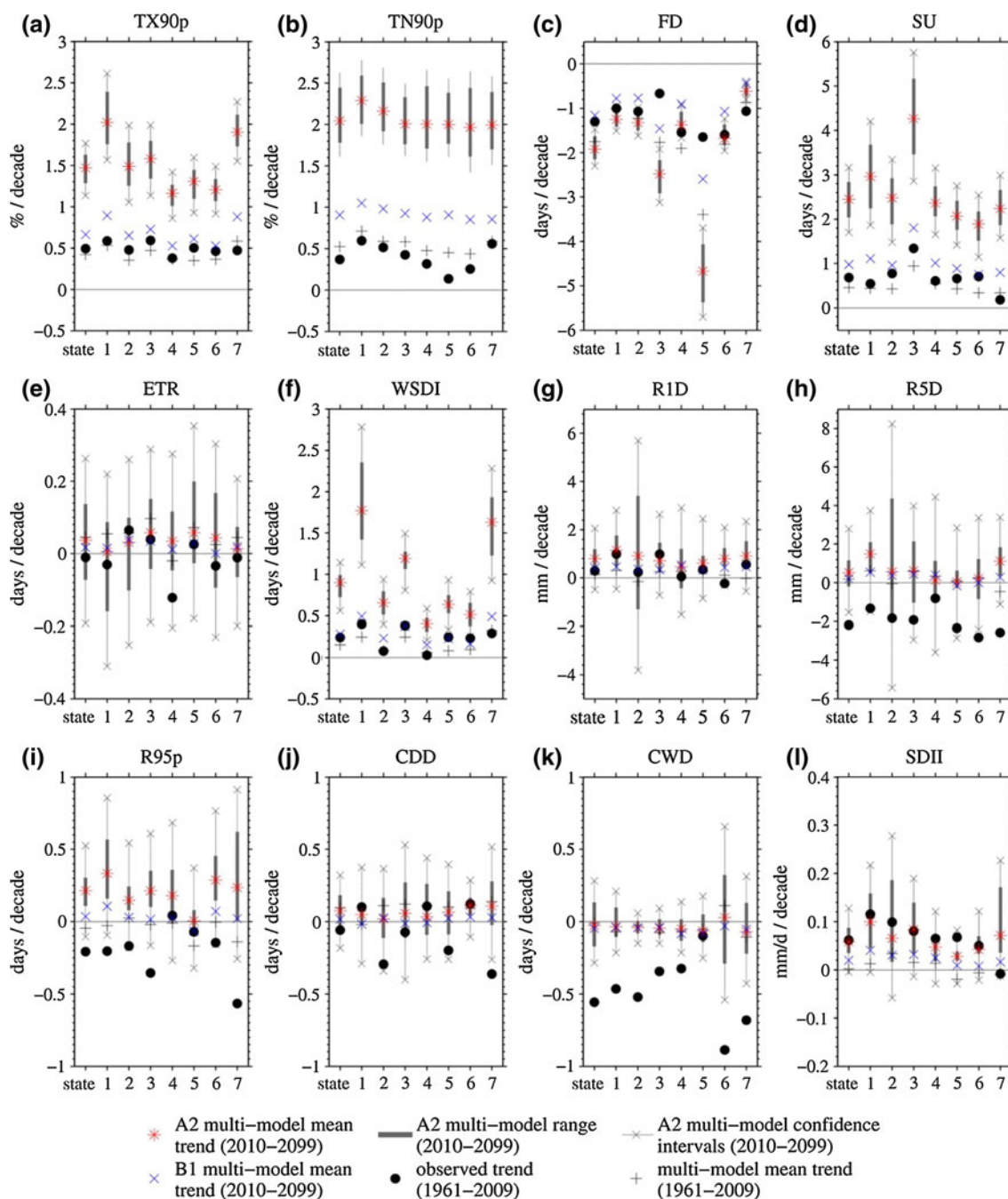


Fig. 9 Statewide and district area-averaged annual decadal trends calculated for the 0.1° AWAP observations (1961–2009) and the 0.1° CCAM simulations multi-model mean (1961–2009 and 2010–2099) for the extreme indices used in this study (definitions shown in Table 1, per decade). CCAM multi-model mean trends (2010–2099

only) are shown with the minimum and maximum spread calculated across the six models (*thick bars*) and with the 90 % confidence interval of the trend (*thin whiskers*) for the SRES A2 scenario. Numbered Tasmania districts (1–7) are defined in Fig. 1b

is smaller than the projected increase of SU (Fig. 8d). The projected changes to SU is distributed across a more extensive areas in the eastern half of the state (Fig. 7d) which suggests an increase in hot pre-frontal north-westerlies and an enhanced Foehn wind effect.

4.2 Future extreme precipitation projections

Projected changes in the extreme precipitation indices are smaller than projected changes in the extreme temperature indices. This reflects the greater internal variability of the

precipitation indices and the relative small net change in precipitation over the entire region. The R1D and R5D indices both show increases statewide of ~ 8 mm for the SRES A2 scenario by the end of the twenty-first century (Fig. 8g, h). Particularly strong increases are projected in late summer and autumn in the east of the state (not shown). The greater increase in R1D (up to 40 %) compared with R5D (~ 25 %) suggests the increasing trend in R5D is due to more intense short-duration events. Indeed, increases in the CCAM–MMM 6-min peak precipitation rate (typically referred to as an instantaneous rate) is particularly strong in late summer, autumn and spring in the eastern half of the state (White et al. 2010b) with a ~ 60 % increase in the East Coast district for the SRES A2 scenario by the end of the century (not shown). A warming troposphere, with greater capacity to hold moisture, is expected to lead to increases in extreme precipitation totals, constrained by the Clausius–Clapeyron relation (Allen and Ingram 2002; Pall et al. 2007; Allan and Soden 2008). Globally, an amplification of precipitation extremes has already been observed and attributed to warming (Min et al. 2011). This global-scale phenomenon can be modulated by regional-scale influences, but the (positive) sign of change in short-duration heavy precipitation in the CCAM projections across Tasmania is almost uniformly consistent with this global-scale effect.

The spatial change in R95p in the CCAM–MMM is for an increase everywhere except over the Central Plateau district (Fig. 7i), and a net statewide increase for the SRES A2 scenario, although there is little change for the SRES B1 scenario (Fig. 8i). The projected increases in the Western district are driven predominantly by the increased frequency of winter events with lesser increases in the autumn and spring seasons, which is consistent with an enhancement of mean westerly circulation over the region in winter (Grose et al. 2012a). The projected changes in CDD and CWD are more modest, showing a statewide trend towards more CDD (Fig. 8j) and less CWD (Fig. 8k) for the SRES A2 scenario. This suggests an overall move to more prolonged dry spells interspaced with an increased frequency of R95p (Fig. 8i).

The projected increase in SDII statewide of ~ 0.5 mm/day for the SRES A2 scenario (Fig. 8l) suggests that increases in daily extreme precipitation totals are likely to be sufficiently high to cause mean annual precipitation totals on wet-days to increase over many areas of Tasmania despite a statewide projected decrease in the number of annual rain days (White et al. 2010b; Grose et al. 2010). The general tendency towards delivery of precipitation from fewer, more intense events as the climate warms is a robust feature of theory, simulations and observations (e.g. Pall et al. 2007; Allan and Soden 2008). This tendency is evident in the CCAM simulations in almost all areas of

Tasmania, except for the Central Plateau district, which has the largest projected decline in mean precipitation (Grose et al. 2010).

4.3 Future decadal trends

Trends of the temperature and precipitation extreme indices are shown in Fig. 9 as statewide area-averages and for each of the seven districts (1–7) defined in Fig. 1b. As with previous sections, the projected trends up to 2099 are calculated independently per model and the results averaged across the six models to provide a central estimate per scenario. The central value of each index is shown with a range determined from the spread of values from minimum and maximum modelled value and with 90 % confidence intervals for the SRES A2 scenario, and significance is tested at the 5 % level using the Mann–Kendall test (Table 4). Decadal trends for the 1961–2009 period, for both the AWAP observations and the CCAM–MMM, together with the projected trend for the SRES B1 scenario up to 2099 are also shown for reference.

Projected statewide area-averaged decadal trends of the extreme temperature indices, TX90p, TN90p, SU, WSDI and FD show increases relative to the validation period, (typically in regions where the mean temperature is higher) under the SRES A2 scenario (Fig. 9a–f; Table 4). There is also strong agreement between the six CCAM simulations of the extreme temperature indices in both the sign and magnitude of the decadal trends with statistically significant trends (at the 5 % level). The exception is ETR which displays mixed signs and trends. Only GFDL-CM2.1 shows a statistically significant trend for ETR for the SRES A2 scenario. More appreciable differences are evident between the statewide area-average trends for the extreme precipitation indices (Fig. 9g–l; Table 4). No single model is found to show consistently biased or outlying values, although UKMO-HadCM3 is the only model to not project any statistically significant trends for the statewide area-averaged precipitation indices and the CSIRO-Mk3.5 simulation shows a slight decreasing trend of CDD and an increasing trend of CWD, which is different to the other CCAM simulations.

In general, the spatial distribution of the projected extreme precipitation trends (Fig. 9) align well with the patterns of projected mean annual precipitation (Grose et al. 2010), with an increase in winter and a decrease in summer in the Western district and projected wetter summers for eastern districts (not shown). Weak CCAM–MMM trends are evident for the Central Plateau district for all of the extreme precipitation indices (Fig. 9g–l), with close agreement between the six CCAM simulations. The CCAM simulations show increased multi-model spread for the longer duration precipitation indices of CDD (Fig. 9j)

and CWD (Fig. 9k), particularly in districts with the highest annual precipitation totals such as the Western district. The East Coast district in contrast shows more uncertainty for RID (Fig. 9g) and R5D (Fig. 9h) totals than any other district, reflecting the high inter-annual variability in this area of Tasmania driven by individual, rare extreme events.

The projected extreme decadal trends up to 2099 of SU (Fig. 9d) and WSDI (Fig. 9f), are substantially greater than observed trends for the 1961–2009 validation period, indicating a progressive increase in hot extremes with a high degree of confidence across the multi-model simulations (Table 4) across all districts. Indices such as RID (Fig. 9g) and SDII (Fig. 9l) show a smaller departure from the observed trends, with more constant trends through the coming century. For other indices however, particularly those that model multi-day events such as CDD (Fig. 9j) and CWD (Fig. 9k), the poorer simulation of the observed trend during the validation period increases the uncertainty around the projected future trends of these indices.

5 Discussion and conclusions

The six global-scale host GCMs used in this study have been previously shown to under-represent extremes due to poor representation of variability across Tasmania (Corney et al. 2010) and limited model resolution. As shown in this study, the downscaling process enables both the regional spatial and seasonal patterns of temperature and precipitation extremes to be simulated with a high level of agreement with the AWAP observations for the 1961–2009 validation period. This can be related to the finer spatial resolution of features such as topography in CCAM, but also the better representation of large-scale climatological features such as location and intensity of the mean mid-latitude westerly jet (Grose et al. 2012a) and frequency of cutoff lows (Grose et al. 2012b). The bias-correction of the SSTs in the parent GCM models used to drive the down-scaled simulations has also ensured that the inputs from each GCM are aligned with observed large-scale temperatures during the validation period and has also significantly contributed to the narrow spread of the downscaled output. While there is no possibility that the parent GCMs can distinguish the influence of regional-scale drivers when Tasmania is typically represented by between 0 and 6 grid cells, the higher resolution of the CCAM simulations have been shown here to simulate distinct regional mechanisms that influence extremes across the different regions of Tasmania. For example, extreme precipitation events in the west of the state are often the result of strong cold fronts interacting with rugged topography, whereas those in the northeast of Tasmania are often the result of intense lows

making landfall, both of which are well represented by the CCAM simulations (Grose et al. 2012b).

Evidence of some persistent spatial errors and biases in the downscaled simulations, of varying strengths in each region and season, are noted however. These include a distinct east–west divide in the simulation of precipitation extremes for the validation period across Tasmania, with a general overestimation in extreme precipitation in the east and an underestimation in the west. Some of these spatial inconsistencies can be attributed to biases in the simulated synoptic-scale meteorology in the models (Grose et al. 2012a), although these tend to fall within the uncertainty of the estimates of the trends and are small relative to the future projected changes. The downscaled simulations demonstrate reduced skill in areas where the most ‘extreme’ extreme values are observed, notably the East Coast and North East districts for extreme precipitation events and the higher-elevation Central Plateau district for cold temperature extremes. They also struggle to simulate events such as the single-most extreme temperature values in any given year, which can be related to an overestimation of warm and cold extremes in some regions. Lower skill is also seen in regions with varied topography and where events are more likely to be driven by localised phenomenon associated with complex systems that cannot be fully resolved by the models.

Both the evident skill and noted deficiencies are reflected in the decadal trends simulated across the down-scaled simulations and influence the ability of the models to simulate the trends of the extreme indices over the validation period. The majority of the models simulate trends that are similar in magnitude and sign to the extremes indices in the AWAP observations, with only the trends in ETR and CDD from the CCAM–MMM not falling within the 95 % confidence intervals of the trends estimated from the AWAP observations. Averaged across Tasmania, observed trends of increased TX90p and TN90p with decreased FD are skilfully captured by the high-resolution models, but in general the simulations of the extreme precipitation indices have lower confidence than the extreme temperature indices. These results are consistent with findings derived from the coarse-resolution GCMs at the global-scale (e.g. Kiktev et al. 2007; Kharin et al. 2007) and across the Australian continent (Alexander and Arblaster 2009). Alexander and Arblaster (2009) find that GCMs are generally able to simulate the observed trends and, to some degree, the range of variability of extremes averaged across Australia. However, due to the limited number of observations over Tasmania in the HadEX observational dataset, Alexander and Arblaster (2009) did not include Tasmania in their assessment (Lisa Alexander and Julie Arblaster, pers comm.).

The level of skill in describing the validation period provides increased confidence that high-resolution simulations have significantly greater capacity to make realistic future projections of extremes at the regional level than do GCMs. The future projections of the extreme temperature indices are consistent with the projected change in mean temperature due to greenhouse warming, with significant increases in TN90p, TX90p and SU. However, spatial variations in the pattern of change indicate that localised influences are also playing a role in some regions, such as an enhanced response in the projected change in WSDI in northern Tasmania compared to the south. For the extreme precipitation indices, the future projected changes appear to be driven primarily by global-scale factors, but with second-order influences from regional drivers and features. There is an almost uniform increase in all indices of extreme precipitation intensities (R1D, R5D, R95p), and a mostly consistent tendency towards shorter rain periods with longer dry spells (SDII, CWD, CDD) over most of Tasmania. This is consistent with an enhanced hydrological cycle influencing the extremes under a warming climate (e.g. Pall et al. 2007), although regional modulation of this overall tendency is seen in the generally weaker or drier projected changes over the Central Plateau district in the centre of Tasmania, which is likely to be related to topography. The north-east of the state displays a pattern of an increasing frequency of extreme precipitation events, although there is reduced consistency across the models in this area.

With regards to the indices themselves, we find that the regional downscaled simulations generally show higher skill at simulating the observed extreme indices that are derived from either percentile-based thresholds (e.g. TN90p, TX90p) or ratios (e.g. SDII) than the exceedance of fixed thresholds (e.g. FD, SU, CDD), suggesting that extreme indices based on percentile values, anomalies or fractional differences relative to a baseline period appear to be more appropriate for projecting changes to extremes.

In conclusion, this study has contributed to the greater understanding of the regional downscaling of climate models in the context of how extremes in temperature and precipitation are represented. It has shown, for the first time, that there are likely to be substantial changes to the characteristics of extreme events across many regions of Tasmania. In particular it has indicated that there are likely to be increases in TX90p, TN90p, SU, R95p, and R1D totals, combined with decreases in FD and CWD with greater uncertainty associated with precipitation extremes compared to temperature extremes. It has also provided valuable insights into the representation of climate extremes by regional climate models.

Acknowledgments The authors would like to acknowledge JL McGregor (CAWCR, CSIRO) for providing the CCAM model and assisting in the running of the regional simulations, and WF Budd (University of Tasmania) for advice in the development of the scientific approach. Many thanks to JC Bennett (CSIRO) and MJ Pook (CAWCR, CSIRO) for comments and suggestions during the drafting of this manuscript, SE Perkins (University of New South Wales) for advice with the PDF skill scores and S Foster (CSIRO) for help with the trend calculations. Thanks also to LV Alexander (University of New South Wales), JM Arblaster (CAWCR, Bureau of Meteorology), and P Fox-Hughes and I Barnes-Keoghan (both Bureau of Meteorology) for their advice during the Climate Futures for Tasmania project, and to two anonymous reviewers for their highly constructive and insightful comments. This work was supported by the Australian Government's Cooperative Research Centres Program through the Antarctic Climate and Ecosystems Cooperative Research Centre (ACE CRC). Climate Futures for Tasmania was possible with support through funding and research of a consortium of state and national partners. We acknowledge the following modelling groups, the Program for Climate Model Diagnosis and Intercomparison (PCMDI) and the WCRP's Working Group on Coupled Modelling (WGCM) for their roles in making available the CMIP3 multi-model dataset.

References

- Alexander LV, Arblaster JM (2009) Assessing trends in observed and modelled climate extremes over Australia in relation to future projections. *Int J Climatol* 29:417–435. doi:10.1002/joc.1730
- Alexander LV, Zhang X, Peterson TC, Caesar J, Gleason B, Klein Tank AMG, Haylock M, Collins D, Trewin B, Rahim F, Tagipour A, Kumar Kolli R, Revadekar JV, Griffiths G, Vincent L, Stephenson DB, Burn J, Aguilar E, Brunet M, Taylor M, New M, Zhai P, Rusticucci M, Vazquez Aguirre JL (2006) Global observed changes in daily climate extremes of temperature and precipitation. *J Geophys Res Atmos* 111: D05109. doi: 10.1029/2005JD006290
- Allan RP, Soden BJ (2008) Atmospheric warming and the amplification of precipitation extremes. *Science* 321:1481–1484. doi: 10.1126/science.1160787
- Allen MR, Ingram WJ (2002) Constraints on future changes in climate and the hydrologic cycle. *Nature* 419:224–232. doi: 10.1038/nature01092
- Bennett JC, Ling FLN, Graham B, Grose MR, Corney SP, White CJ et al (2010) Climate futures for Tasmania: water and catchments technical report. Antarctic Climate and Ecosystems Cooperative Research Centre, Hobart
- Bennett JC, Ling FLN, Post DA, Grose MR, Corney SP et al (2012) High-resolution projections of surface water availability for Tasmania, Australia. *Hydrol Earth Syst Sci* 16:1287–1303
- Berbery EH, Fox-Rabinovitz MS (2003) Multiscale diagnosis of the North American monsoon system using a variable-resolution GCM. *J Clim* 16:1929–1947
- Berg P, Haerter JO, Thejll P, Piani C, Hagemann S, Christensen JH (2009) Seasonal characteristics of the relationship between daily precipitation intensity and surface temperature. *Geophys Res Lett* 114:D18102. doi:10.1029/2009JD012008
- Boé J, Terray L (2007) A weather-type approach to analyzing winter precipitation in France: twentieth-century trends and the role of anthropogenic forcing. *J Clim* 21:3118–3133
- Bureau of Meteorology (2012) Rainfall and temperature extremes. Bureau of Meteorology. <http://www.bom.gov.au/climate/extreme/records.shtml>. Accessed 24 July 2012
- Burton I, Dube OP, Campbell-Lendrum D, Davis I, Klein RJT, Linnerooth-Bayer J, Sanghi A, Toth F (2012) Managing the

- risks: international level and integration across scales. In: Field CB, Barros V et al (eds) *Managing the risks of extreme events and disasters to advance climate change adaptation A special report of working groups I and II of the intergovernmental panel on climate change*. Cambridge University Press, Cambridge and New York, pp 393–435
- Cai W, Shi G, Cowan T, Bi D, Ribbe J (2005) The response of the Southern annular mode, the East Australian current, and the southern mid-latitude ocean circulation to global warming. *Geophys Res Lett* 32:L23706. doi:[10.1029/2005GL024701](https://doi.org/10.1029/2005GL024701)
- Chiew FHS, Kirono DGC, Kent DM, Frost AJ, Charles SP et al (2010) Comparison of runoff modelled using rainfall from different downscaling methods for historical and future climates. *J Hydrol* 387:10–23
- Christensen JH, Hewitson B, Busuioc A, Chen A, Gao X, Held I, Jones R, Kolli RK, Kwon WT, Laprise R, Magaña Rueda V, Mearns L, Menéndez CG, Räisänen J, Rinke A, Sarr A, Whetton P (2007) Regional climate projections. In: Solomon SD, Qin M, Manning Z, Chen M, Marquis KB, Averyt M, Tignor, Miller HL (eds). *Climate change: the physical science basis. Contribution of working group I to the fourth assessment report of the intergovernmental panel on climate change*. Cambridge University Press, Cambridge and New York
- Collins DA, Della-Marta PM, Plummer N, Trewin BC (2000) Trends in annual frequencies of extreme temperature events in Australia. *Aust Meteorol Mag* 49:277–292
- Corney SP, Katzfey JF, McGregor JL, Grose MR, White CJ et al (2010) *Climate futures for Tasmania: climate modelling technical report*. Antarctic Climate and Ecosystems Cooperative Research Centre, Hobart
- Dai A, Trenberth KE, Karl TR (1999) Effects of clouds, soil moisture, precipitation, and water vapor on diurnal temperature range. *J Clim* 12:2451–2473
- Dole R, Hoerling M, Perlwitz J, Eischeid J, Pegion P, Zhang T, Quan X-W, Xu T, Murray D (2011) Was there a basis for anticipating the 2010 Russian heat wave? *Geophys Res Lett* 38:L06702. doi:[10.1029/2010GL046582](https://doi.org/10.1029/2010GL046582)
- Dommenget D (2009) The ocean's role in continental climate variability and change. *J Clim* 22:4939–4952
- Donat MG, Alexander LV (2012) The shifting probability distribution of global daytime and night-time temperatures. *Geophys Res Lett* 39:L14707. doi:[10.1029/2012GL052459](https://doi.org/10.1029/2012GL052459)
- Engelbrecht FA, McGregor JL, Engelbrecht CJ (2009) Dynamics of the confor-mal-cubic atmospheric model projected climate-change signal over southern Africa. *Int J Climatol* 29:1013–1033
- Fox-Hughes P (2008) A fire danger climatology for Tasmania. *Aust Met Mag* 57:109–120
- Fox-Rabinovitz MS, Cote J, Deque M, Dugas B, McGregor JL (2006) Variable-resolution GCMs: stretched-grid model intercomparison project (SGMIP). *J Geophys Res* 111:D16104. doi:[10.1029/2005JD006520](https://doi.org/10.1029/2005JD006520)
- Gallant A, Hennessy K, Risbey J (2007) Trends in precipitation indices for six Australian regions: 1910–2005. *Aust Meteorol Mag* 56:223–239
- Grose MR, Barnes-Keoghan I, Corney SP, White CJ, Holz GK et al (2010) *Climate futures for Tasmania: general climate impacts*. Antarctic Climate and Ecosystems Cooperative research Centre, Hobart
- Grose MR, Corney SP, Bennett JC, White CJ, Holz GK et al (2012a) A regional response in mean westerly circulation and rainfall to projected climate warming over Tasmania, Australia. *Clim Dyn* online first. doi:[10.1007/s00382-012-1405-1](https://doi.org/10.1007/s00382-012-1405-1)
- Grose MR, Pook MJ, McIntosh PC, Risbey JS, Bindoff NL (2012b) The simulation of cutoff lows in a regional climate model: reliability and future trends. *Clim Dyn* online first. doi:[10.1007/s00382-012-1368-2](https://doi.org/10.1007/s00382-012-1368-2)
- Hansen J, Sato M, Ruedy R (2012) Perception of climate change. *P Natl Acad Sci USA* 109(37):E2415–E2423. doi:[10.1073/pnas.1205276109](https://doi.org/10.1073/pnas.1205276109)
- Hegerl GC, Zwiers FW, Stott PA, Kharin VV (2004) Detectability of anthropogenic changes in annual temperature and precipitation extremes. *J Clim* 17:3683–3700
- IPCC (2012) *Managing the risks of extreme events and disasters to advance climate change adaptation*. In: Field CB, Barros V, Stocker TF, Qin D, Dokken DJ, Ebi KL, Mastrandrea MD, Mach KJ, Plattner G-K, Allen SK, Tignor M, Midgley PM (eds) A special report of working groups I and II of the Intergovernmental panel on climate change. Cambridge University Press, Cambridge and New York, p 582
- Jones DA, Wang W, Fawcett R (2009) High-quality spatial climate data-sets for Australia. *Aust Meteorol Oceanogr J* 58:233–248
- Katzfey JJ, McInnes KL (1996) GCM simulations of eastern Australian cutoff lows. *J Clim* 9:2337–2355
- Katzfey JJ, McGregor JL, Nguyen KC, Thatcher M (2009) Dynamical downscaling techniques: impacts on regional climate change signals. *World IMACS/MODSIM Congress*, Cairns, pp 2377–2383
- Kendall MG (1975) *Rank correlation methods*. Griffin, London
- Kendon EJ, Rowell DP, Jones RG (2010) Mechanisms and reliability of future projected changes in daily precipitation. *Clim Dyn* 35:489–509
- Kharin VV, Zwiers FW, Zhang X, Hegerl GC (2007) Changes in temperature and precipitation extremes in the IPCC ensemble of global coupled model simulations. *J Clim* 20:1419–1444
- Kiktev D, Caesar J, Alexander LV, Shiogama H, Collier M (2007) Comparison of observed and multimodeled trends in annual extremes of temperature and precipitation. *Geophys Res Lett* 34:L10702. doi:[10.1029/2007GL029539](https://doi.org/10.1029/2007GL029539)
- King AD, Alexander LV, Donat MG (2012) The efficacy of using gridded data to examine extreme rainfall characteristics: a case study for Australia. *Int J Climatol* advanced online publication. doi:[10.1002/joc.3588](https://doi.org/10.1002/joc.3588)
- Lal M, McGregor JL, Nguyen KC (2008) Very high-resolution climate simulation over Fiji using a global variable-resolution model. *Clim Dyn* 30:293–305
- Mann HB (1945) Nonparametric trends against test. *Econometrica* 13:245–259
- McGregor JL (2005) *C-CAM: Geometric aspects and dynamical formulation*. CSIRO Atmospheric Research Technical Paper 43
- McGregor JL, Dix MR (2008) An updated description of the confor-mal-cubic atmospheric model. In: Hamilton K, Ohfuchi W (eds) *High resolution simulation of the atmosphere and ocean*. Springer, Berlin, pp 51–76
- McIntosh P, Pook M, Risbey J, Hope P, Wang G, Alves OA (2008) *Final report—Australia's regional climate drivers*. Centre for Australian Weather and Climate Research, CSIRO
- Meehl GA, Tebaldi C, Nychka D (2004) Changes in frost days in simulations of 21st century climate. *Clim Dyn* 23:495–511
- Meehl GA, Covey AC, Delworth T, Latif M, McAvaney BJ, Mitchell JFB, Stouffer RJ, Taylor KE (2007a) The WCRP CMIP3 multi-model dataset: a new era in climate change research. *Bull Am Meteor Soc* 88:1383–1394
- Meehl GA, Stocker TF, Collins WD, Friedlingstein P, Gaye AT, Gregory JM, Kitoh A, Knutti R, Murphy JM, Noda A, Raper SCB, Watterson IG, Weaver AJ, Zhao Z-C (2007b) Global climate projections. In: Solomon S, Qin D, Manning M et al (eds) *Climate change: the physical science basis contribution of working group I to the fourth assessment report of the intergovernmental panel on climate change*. Cambridge University Press, Cambridge and New York
- Mills G (2005) On the subsynoptic-scale meteorology of two extreme fire weather days during the Eastern Australian fires of January 2003. *Aust Meteorol Mag* 54:265–290

- Min S-K, Zhang X, Zwiers FW, Hegerl GC (2011) Human contribution to more-intense precipitation extremes. *Nature* 470:378–381. doi:[10.1038/nature09763](https://doi.org/10.1038/nature09763)
- Murphy BF, Timbal B (2008) A review of recent climate variability and climate change in southeastern Australia. *Int J Climatol* 28:859–879. doi:[10.1002/joc.1627](https://doi.org/10.1002/joc.1627)
- Nakićenović N, Swart R (2000) Special report on emissions scenarios. A special report of working group III of the Intergovernmental panel on climate change. Cambridge University Press, Cambridge
- Nguyen KC, McGregor JL (2009) Modelling the Asian summer monsoon using CCAM. *Clim Dyn* 32:219–236
- Nguyen KC, Katzfey JJ, McGregor JL (2011) Global 60 km simulations with CCAM: evaluation over the tropics. *Clim Dyn* online first. doi:[10.1007/s00382-011-1197-8](https://doi.org/10.1007/s00382-011-1197-8)
- Pall P, Allen MR, Stone DA (2007) Testing the Clausius–Clapeyron constraint on changes in extreme precipitation under CO2 warming. *Clim Dyn* 28:351–363. doi:[10.1007/s00382-006-0180-2](https://doi.org/10.1007/s00382-006-0180-2)
- Pall P, Aina T, Stone DA, Stott PA, Nozawa T, Hilberts AG, Lohmann D, Allen MR (2011) Anthropogenic greenhouse gas contribution to flood risk in England and Wales in autumn 2000. *Nature* 470:382–385
- Perkins SE, Pitman AJ, Holbrook NJ, McAneney J (2007) Evaluation of the AR4 climate models' simulated daily maximum temperature, minimum temperature and precipitation over Australia using probability density functions. *J Clim* 20:4356–4376
- Peterson TC, Stott PA, Herring S (2012) Explaining extreme events of 2011 from a climate perspective. *Bull Am Meteor Soc* 93:1041–1067. doi:[10.1175/BAMS-D-12-00021.1](https://doi.org/10.1175/BAMS-D-12-00021.1)
- Pook MJ, Risbey J, McIntosh P (2010) East coast lows, atmospheric blocking and rainfall: a Tasmanian perspective. *IOP Conf Ser: Earth Environ Sci* 11:012011
- Randall DA, Wood R, Bony S, Colman R, Fichetef T et al (2007) Climate models and their evaluation. In: Solomon S, Qin D, Manning M et al (eds) *Climate change 2007: the physical science basis*. Contribution of working group I to the fourth assessment report of the intergovernmental panel on climate change. Cambridge University Press, Cambridge and New York
- Raupach MR, Briggs PR, Haverd V, King EA, Paget M, Trudinger CM (2008) Australian water availability project (AWAP): final report for phase 3. CSIRO Marine and Atmospheric Research, Canberra, p 67
- Scaife AA, Folland CK, Alexander LV, Moberg A, Knight JR (2008) European climate extremes and the North Atlantic Oscillation. *J Clim* 21:72–83
- Schiermeier Q (2011) Extreme measures. *Nature* 477:148–149. doi:[10.1038/477148a](https://doi.org/10.1038/477148a)
- Seneviratne SI, Nicholls N, Easterling D, Goodess CM, Kanae S, Kossin S, Luo Y, Marengo J, McInnes K, Rahimi M, Reichstein M, Sorteberg A, Vera C, Zhang X (2012) Changes in climate extremes and their impacts on the natural physical environment. In: Field CB, Barros V et al (eds) *Managing the risks of extreme events and disasters to advance climate change adaptation*. A special report of working groups I and II of the Intergovernmental panel on climate change. Cambridge University Press, Cambridge and New York, pp 109–230
- Sillmann J, Roekner E (2008) Indices for extreme events in projections of anthropogenic climate change. *Clim Change* 86:83–104
- Smith I, Chandler E (2009) Refining rainfall projections for the Murray Darling Basin of south-east Australia—the effect of sampling model results based on performance. *Clim Change* 102:377–393
- Solomon S, Qin D, Manning M, Alley RB, Berntsen T, Bindoff NL, Chen Z, Chidthaisong A, Gregory JM, Hegerl GC, Heimann M, Hewitson B, Hoskins BJ, Joos F, Jouzel J, Kattsov V, Lohmann U, Matsuno T, Molina M, Nicholls N, Overpeck J, Raga G, Ramaswamy V, Ren J, Rusticucci M, Somerville R, Stocker TF, Whetton P, Wood RA, Wratt D (2007) Technical summary. In: Solomon S, Qin D, Manning M, Chen Z, Marquis M, Averyt KB, Tignor M, Miller HL (eds) *Climate change 2007 the physical science basis*. Contribution of working group I to the fourth assessment report of the intergovernmental panel on climate change. Cambridge University Press, Cambridge and New York
- Suppiah R, Hennessy KJ, Whetton PH, McInnes KL, Macadam I, Bathols J, Ricketts J (2007) Australian climate change scenarios derived from simulations performed for the IPCC 4th assessment report. *Aust Meteorol Mag* 56:131–152
- Tebaldi C, Hayhoe K, Arblaster JM, Meehl GA (2006) Going to the extremes: an intercomparison of model-simulated historical and future changes in extreme events. *Clim Change* 79:185–211
- Thatcher M, McGregor JL (2009) Using a scale-selective filter for dynamical downscaling with the conformal cubic atmospheric model. *Mon Weather Rev* 137:1742–1752
- Thatcher M, McGregor JL (2011) A technique for dynamically downscaling daily-averaged GCM datasets using the conformal cubic atmospheric model. *Mon Weather Rev* 139:79–95
- van Oldenborgh GJ, Philip SY, Collins M (2005) El Niño in a changing climate: a multi-model study. *Ocean Sci* 1:81–95. doi:[10.5194/os-1-81-2005](https://doi.org/10.5194/os-1-81-2005)
- Watterson IG, McGregor JL, Nguyen KC (2008) Changes in extreme temperatures of Australasian summer simulated by CCAM under global warming, and the roles of winds and land-sea contrasts. *Aust Meteorol Mag* 57:195–212
- White CJ, Sanabria LA, Corney SP, Grose MR, Holz GK et al (2010a) Modelling extreme events in a changing climate using regional dynamically-downscaled climate projections. IEMSs 2010 International Congress on Environmental Modelling and Software, Ottawa
- White CJ, Grose MR, Corney SP, Bennett JC, Holz GK et al (2010b) Climate futures for Tasmania: extreme events technical report. Antarctic Climate and Ecosystems Cooperative Research Centre, Hobart
- Zhang X, Alexander L, Hegerl GC, Jones P, Klein Tank A, Peterson TC, Trewin B, Zwiers FW (2011) Indices for monitoring changes in extremes based on daily temperature and precipitation data. *WIREs Clim Change* 2:851–870. doi:[10.1002/wcc.147](https://doi.org/10.1002/wcc.147)